9950-1064

Contract NAS5-3756

ASTRO

RESEARCH CORPORATION

FINAL REPORT

A STUDY OF STRUCTURAL CONCEPTS FOR ULTRALIGHTWEIGHT SPACECRAFT

by
Richard K. Miller,
Karl Knapp
John M. Hedgepeth

ARC-TN-1127

16 April 1984

Prepared for
Jet Propulsion Laboratory
under Contract No. 956386

This report was prepared for the Jet Propulsion Laboratory, California Institute of Technology, sponsored by the National Aeronautics and Space Administration.

Prepared by

Astro Research Corporation
6390 Cindy Lane
Carpinteria, California 93013

TABLE OF CONTENTS

SECTION 1: INTRODUCTION 1-1

SECTION 2: DESIGN OF A SPINNING REFLECTOR SPACECRAFT 2-1

2.1 Design of Membrane Reflector 2-1
2.2 Design of Outer Rim Mass 2-8
2.3 Design of Front Stays 2-9
2.4 Design of Back Stays 2-10
2.5 Design of Inflated Cylindrical Center Column 2-11
2.6 Design of Truss Center Column 2-15
2.6.1 Design of a Truss Column Including Effects of Initial Imperfections 2-18
2.6.2 Design of a Perfect Truss Column 2-21
2.6.3 Design of a Minimum Weight, Perfect Truss Column 2-23
2.7 Effects of an Attitude Control System on Column Design 2-26
2.8 Satellite Mass Moment of Inertia Ratios 2-30

SECTION 3: DESIGN OF A TRUSS-SUPPORTED PARABOLOIDAL REFLECTOR SPACECRAFT 3-1

3.1 Design of a Deep Truss Paraboloidal Reflector 3-1
3.1.1 Slenderness Requirements on Truss Members 3-5
3.1.2 Requirement 1 - Horizontal Testing 3-5
3.1.3 Requirement 2 - Vertical Testing 3-7
3.1.4 Requirement 3 - Fabrication Tolerances 3-7
3.1.5 Requirement 4 - Built-In Loads Due to Member Length Errors 3-7
3.1.6 Requirement 5 - Member Vibration Frequencies 3-8
3.2 Design of a Geodesic Dome Paraboloidal Reflector 3-8
3.3 Design of a Ring Stiffener for the Geodesic Dome Reflector 3-10
3.4 Parametric Mass Relations for the Tetrahedral Truss and Geodesic Dome Support Structures 3-14
3.5 Design of a Tripod Support Structure for the Paraboloidal Reflector Feed 3-17
3.6 Design of a Paraboloidal Tetrahedral Truss Reflector with Inflated Struts 3-21

SECTION 4: MASS SUMMARY AND COMPARISON OF DESIGNS 4-1

4.1 Mass Summary for an Inflated Reflector Spacecraft 4-1
4.1.1 Membrane 4-7
4.1.2 Pressurant 4-7
4.1.3 Deep-Arc Tendons 4-8
4.1.4 Inflated Rim 4-8
4.1.5 Strengths and Weaknesses of the Design 4-9

TABLE OF CONTENTS (concluded)

4.2 Mass Summary of a Spinning Reflector Spacecraft 4-9
4.2.1 Membrane 4-9
4.2.2 Outer Rim Mass 4-9
4.2.3 Front and Back Stays 4-10
4.2.4 Inflated Center Column 4-11
4.2.5 Strengths and Weaknesses of the Design 4-11
4.3 Mass Summary for a Truss Reflector Spacecraft 4-12
4.3.1 Tetrahedral Truss 4-12
4.3.2 Geodesic Dome 4-12
4.3.3 Ring Stiffener 4-12
4.3.4 Mesh/Membrane 4-13
4.3.5 Tripod 4-13
4.3.6 Strengths and Weaknesses of the Design 4-13

APPENDIX: VIBRATIONS OF A SHALLOW DOME A-1

LIST OF TABLES AND FIGURES

Table 2-1. Inflated Cylindrical Center Column Designs 2-14

Table 2-2. Imperfect Truss Column Designs 2-22

Table 2-3. Perfect Truss Column Designs 2-24

Table 2-4. Minimum Weight Perfect Truss Column Designs 2-25

Table 2-5. Comparison of Satellite Fundamental Frequency and Spin Rate for CMG-Controlled Spacecraft 2-29

Table 2-6. Designs for Inflated Cylindrical Column in Attitude-Controlled Spacecraft 2-31

Table 2-7. Mass Moment of Inertia for Spinning Paraboloidal Reflector Spacecraft 2-32

Table 3-1. Paraboloidal Tetrahedral Truss Designs 3-6

Table 3-2. Paraboloidal Geodesic Dome Designs 3-11

Table 3-3. Ring-Stiffener Designs 3-15

Table 3-4. Summary of Tripod Strength, Flexibility, and Mass Characteristics 3-22

Table 4-1. Comparison of Structural Masses of Three Paraboloidal Reflector Spacecraft Configurations 4-6

Figure 2-1. Geometry of spinning paraboloidal membrane 2-2

Figure 2-2. Detailed geometry of connections between major structural components of spinning reflector satellite 2-6

Figure 2-3. Inflated cylindrical center column 2-12

Figure 2-4. S-3 Astromast instrument boom 2-16

Figure 2-5. Twelve-inch Astromast with round longerons and dual fiberglass diagonals and battens 2-17

Figure 2-6. Counter-rotating flywheel attitude control system for spinning reflector spacecraft 2-27

Figure 2-7. Cantilevered beam-column with tip mass model for fundamental vibration frequency of satellite in Figure 2-6 2-28

Figure 3-1. Tetrahedral truss configuration 3-2

Figure 3-2. Geodesic dome configuration 3-9

Figure 3-3. Cross-sectional view of ring stiffener and edge of geodesic dome 3-13

Figure 3-4. Unit mass vs. mesh tension for truss support structures, solid tube designs 3-18

LIST OF TABLES AND FIGURES (concluded)

Figure 3-5. Tripod feed support structure 3-19

Figure 3-6. Tripod column/reflector surface interface 3-20

Figure 4-1. Geometry of cone-paraboloid reflector spacecraft 4-2

Figure 4-2. Pressurized isotensoid strut used in segmented compression rim of inflated cone/paraboloid reflector 4-3

Figure 4-3. Detail of load path between membrane and rim attachment points for inflated reflector configuration 4-4

SECTION 1
INTRODUCTION

This report includes the results of a study conducted by Astro Research Corporation (Astro) on structural concepts for ultralightweight spacecraft as a part of Jet Propulsion Laboratory (JPL) Contract No. 956386. This work is the continuation of studies begun under JPL Contract No. 955873 (Refs. 1-1 and 1-2). The objectives of these studies were to identify and evaluate concepts for ultralightweight space structures and to assess the validity of their potential application in advanced spacecraft.

In the earlier program, the following topics were investigated and reported on:

- o Membrane wrinkling under pretensioning
- o Load-carrying capability of pressurized tubes
- o Equilibrium of a precompressed rim
- o Design of an inflated reflector spacecraft
- o General instability of a rim
- o Structural analysis of a pressurized isotensoid column

In the current study, the design approaches for a paraboloidal reflector spacecraft have been extended to include a spin-stiffened design, including both inflated and truss central columns, and to include both deep truss and rim-stiffened geodesic designs. The spinning spacecraft analysis is included in Section 2. The two truss designs are covered in Section 3 and the Appendix.

Section 4 of this report compares the performance of four different approaches to the structural design of a paraboloidal reflector spacecraft. The spinning and inflated configurations result in very low total masses and some concerns about their performance due to unresolved questions about dynamic stability and lifetimes, respectively.

REFERENCES

1-1. Miller, Richard K.; Adams, Louis R.; and Hedgepeth, John M.: Structural Concepts for Ultralightweight Spacecraft. Astro Research Corporation, ARC-TN-1104, 1 June 1981.

1-2. Final Report - A Study of Structural Concepts for Ultralightweight Spacecraft. Astro Research Corporation, ARC-TN-1114, 14 July 1982.

SECTION 2

DESIGN OF A SPINNING REFLECTOR SPACECRAFT

Reported in this section are the design procedures used to develop the dimensions and masses of spacecraft structural components for a spinning paraboloidal membrane reflector in a hoop-and-column configuration. A primary structural member in this configuration is the compression-carrying central column. Both inflated cylindrical and truss column designs are presented in some detail, but the inflated column is found to be vastly superior on the basis of a total mass criterion.

2.1 DESIGN OF MEMBRANE REFLECTOR

Consider a spinning paraboloidal membrane with coordinates shown in Figure 2-1. As shown in Reference 2-1, the meridional edge tension N_ϕ and circumferential edge tension N_θ may be expressed as

$$N_\phi = \frac{4fP}{\pi D} \frac{\sqrt{1 + (1/16f^2)(2r/D)^2}}{(2r/D)^2} \tag{2-1}$$

$$N_\theta = \frac{m''\omega^2 D^2}{4}\left(\frac{2r}{D}\right)^2 - \frac{4fP}{\pi D} \frac{1}{(2r/D)^2\sqrt{1 + (1/16f^2)(2r/D)^2}} \tag{2-2}$$

where

P = total axial compression force in central column (N)

r = radial coordinate of point on membrane surface (m)

F = focal length of paraboloid (m)

m" = mass per unit area of membrane material (kg/m^2)

ω = circular spin rate (rad/s)

D = diameter of membrane rim (m)

f = F/D

$$Z = \frac{r^2}{4F}$$

(F = focal length)

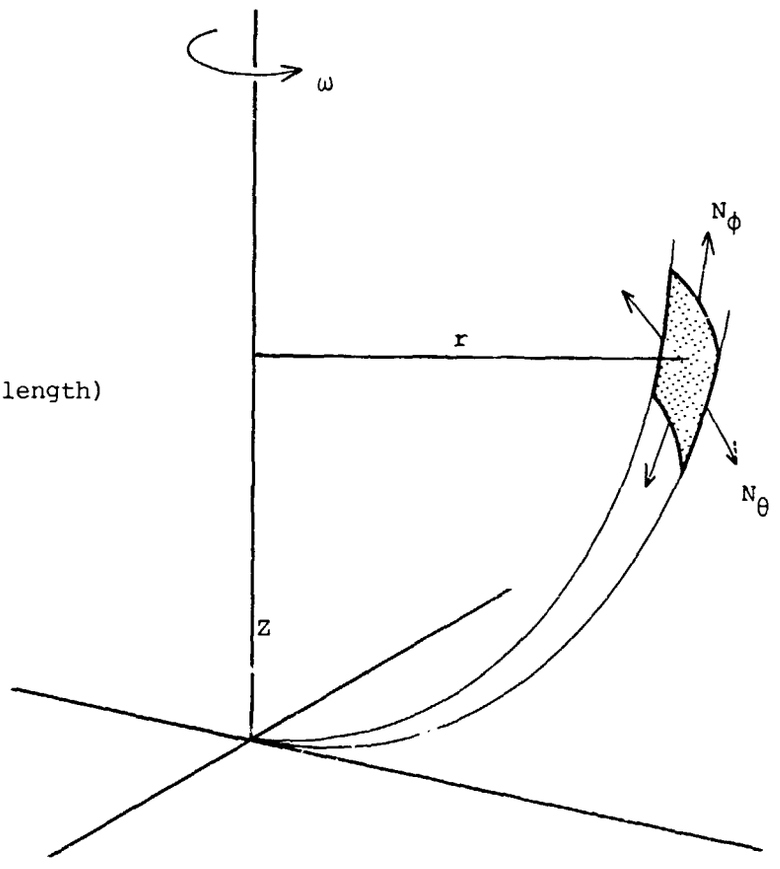

Figure 2-1. Geometry of spinning paraboloidal membrane. *103A*

Note from Eqs. (2-1) and (2-2) that as $(2r/D)\to 0$, we find that $N_\phi \to \infty$ and $N_\theta \to -\infty$. Hence, the central portion of the membrane contains stress singularities and must be removed. The remaining membrane forms a useable reflector surface in the form of a paraboloidal annulus. Let the inner radius r_0 be chosen (arbitrarily) as

$$r_0 = 0.4\left(\frac{D}{2}\right) \qquad (2-3)$$

This choice of r_0 leaves approximately 84 percent of the potential membrane surface for use as a reflector while eliminating the stress singularities in the center.

Note also from Eq. (2-1) that for a membrane of fixed geometry the amplitude of the meridional edge tension is determined by P, and that the maximum value of N_ϕ occurs at r_0. Hence, setting (arbitrarily) this maximum N_ϕ at

$$N_\phi(r = r_0) = 5 \text{ N/m} \qquad (2-4)$$

we can determine the corresponding column compression load P by

$$P = \frac{\pi D(5 \text{ N/m})}{25\, f \sqrt{1 + (1/10f)^2}} \qquad (2-5)$$

Specifically, for three different values of f, Eq. (2-5) yields the results

$$\frac{P}{D} = \begin{cases} 1.23 \text{ N/m}; & f = 1/2 \\ 0.625 \text{ N/m}; & f = 1 \\ 0.315 \text{ N/m}; & f = 2 \end{cases} \qquad (2-6)$$

As revealed by Eq. (2-1), N_ϕ decreases monotonically as r is increased until the minimum value is attained at the outer rim, $r = D/2$. Using the values for column compression P given in Eq. (2-6), we find the corresponding values of the minimum N_ϕ are

$$N_\phi\left(r = \frac{D}{2}\right) = \begin{cases} 0.882 \text{ N/m}; & f = 1/2 \\ 0.821 \text{ N/m}; & f = 1 \\ 0.804 \text{ N/m}; & f = 2 \end{cases} \tag{2-7}$$

Returning to Eq. (2-2), we see that for a membrane of fixed geometry and with fixed column compression P, the amplitude of the circumferential edge tension N_θ is determined by the spin rate ω. Furthermore, N_θ increases with r to attain a maximum value at the outer rim, r = D/2. The minimum value which occurs at the inner rim ($r = r_0$) may be either positive (tensile) or negative (compressive) depending on the size of ω. Since compressive stresses cannot develop in a membrane surface, we arbitrarily set the minimum value of N_θ at

$$N_\theta(r = r_0) = 0.85 \text{ N/m} \tag{2-8}$$

The corresponding spin rate ω is determined by

$$\omega = \left\{\frac{25}{m''D^2}\left[(0.85 \text{ N/m}) + \frac{(5 \text{ N/m})}{1 + (1/10f)^2}\right]\right\}^{1/2} \tag{2-9}$$

Using a membrane unit mass of

$$m'' = 4 \text{ gm/m}^2 \tag{2-10}$$

consistent with a membrane material of Kapton polymer film of thickness 2×10^{-6} m, and mass density of 2×10^3 kg/m^3 (as used in Ref. 2-2), we find specific values of ω for different values of f are

$$\omega D = \begin{cases} 188 \text{ m/s}; & f = 1/2 \\ 190 \text{ m/s}; & f = 1 \\ 191 \text{ m/s}; & f = 2 \end{cases} \tag{2-11}$$

From Eq. (2-^), it is seen that N_θ increases monotonically from $r = r_0$ to attain its maximum value at r = D/2. Using the values for P, m", and ω given in Eqs. (2-6), (2-10), and (2-11), we obtain the following specific values for $N_{\theta max}$

$$N_\theta\left(r = \frac{D}{2}\right) = \begin{cases} 34.6 \text{ N/m}; & f = 1/2 \\ 35.3 \text{ N/m}; & f = 1 \\ 35.6 \text{ N/m}; & f = 2 \end{cases} \tag{2-12}$$

The surface area of the paraboloidal annulus is found from calculus to be

$$\left(\frac{\text{Area}}{\pi D^2/4}\right)_{\text{parab. annulus}} = \begin{cases} 0.899; & f = 1/2 \\ 0.855; & f = 1 \\ 0.844; & f = 2 \end{cases} \tag{2-13}$$

Multiplying the surface area in Eq. (2-13) by the unit mass in Eq. (2-10), we find the total mass of the paraboloidal annulus is

$$\left(\frac{\text{Mass}}{\pi D^2/4}\right)_{\text{parab. annulus}} = \begin{cases} 3.60 \text{ g/m}^2; & f = 1/2 \\ 3.42 \text{ g/m}^2; & f = 1 \\ 3.38 \text{ g/m}^2; & f = 2 \end{cases} \tag{2-14}$$

Since the inner edge of the paraboloidal annulus is not stress free, an additional load-carrying structural element is required inside the inner rim. To enhance the reflective potential of the entire surface, consider a conical membrane whose geometry is chosen as a "best-fit" to the missing paraboloid in the inner region $r < r_0$. In order to reduce the stresses within the conical membrane, additional support is provided by stay tapes which attach at the cone-paraboloid interface and run behind the cone to the end of the central column, as shown in Figure 2-2.

Minimizing the mean-squared vertical deviation between the cone and paraboloid in the region $r < r_0$, we obtain by calculus the optimal choice of Δ

$$\frac{\Delta}{D} = \frac{1}{400\ f} \tag{2-15}$$

Using this value for Δ, we find by calculus the surface area of the interior cone is

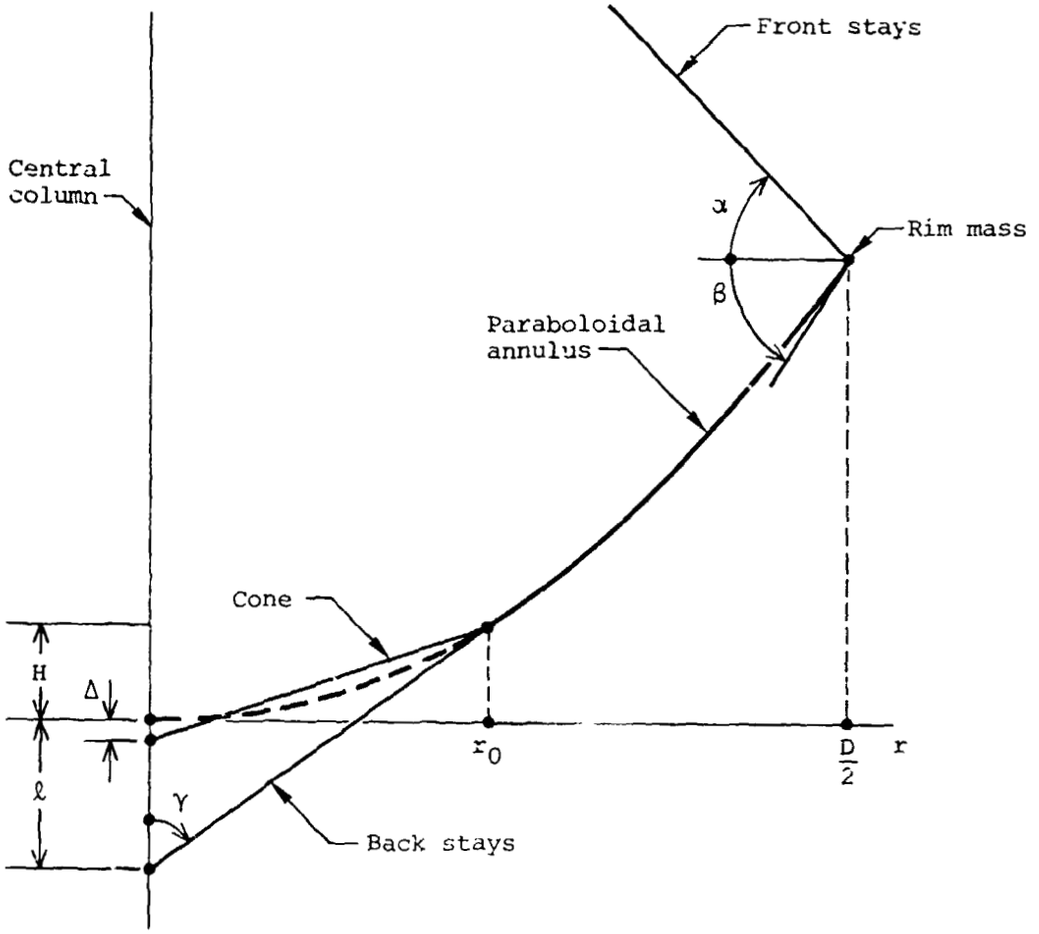

Figure 2-2. Detailed geometry of connections between major structural components of spinning reflector satellite. *104A*

$$\left(\frac{\text{Area}}{\pi D^2/4}\right)_{\substack{\text{interior}\\ \text{cone}}} = \frac{4}{25}\sqrt{1+\left(\frac{1}{16\,f}\right)^2} = \begin{cases} 0.161; & f = 1/2 \\ 0.160; & f = 1 \\ 0.160; & f = 2 \end{cases} \tag{2-16}$$

Multiplying the surface area in Eq. (2-16) by the unit mass in Eq. (2-10), we obtain the total mass of the interior cone

$$\left(\frac{\text{Mass}}{\pi D^2/4}\right)_{\substack{\text{interior}\\ \text{cone}}} = \begin{cases} 0.644\ g/m^2; & f = 1/2 \\ 0.640\ g/m^2; & f = 1 \\ 0.640\ g/m^2; & f = 2 \end{cases} \tag{2-17}$$

Combining the masses of the paraboloidal annulus and interior cone, we obtain the total membrane mass

$$\left(\frac{\text{Mass}}{\pi D^2/4}\right)_{\text{total membrane}} = \begin{cases} 4.24\ g/m^2; & f = 1/2 \\ 4.06\ g/m^2; & f = 1 \\ 4.02\ g/m^2; & f = 2 \end{cases} \tag{2-18}$$

The interior conical membrane is subjected to substantial edge tension, and, in addition, it is spinning and is subjected to centrifugal loads due to its own inertia. Ignoring the centrifugal loads in comparison with the meridional edge tension, we can see that

$$\frac{N_\phi(r)}{N_\phi(r_0)} = \frac{r_0}{r} \tag{2-19}$$

in the cone. The circumferential stress N_θ is negligible in this case. Note that, again, we observe a stress singularity at $r = 0$. Thus, it is again necessary to define another inner radius r_c and remove the membrane in the region $r < r_c$. A conical annulus is formed thereby.

In order to define r_c, let $N_\phi(r_0) = 2.5$ N/m in the cone (the other 2.5 N/m to be carried by the back stays). Then solving from Eq. (2-19) for that radius r_c for which $N_\phi(r_c) = 35$ N/m, we obtain

$$r_c = \frac{D}{70} \tag{2-20}$$

This particular choice of r_c balances the maximum edge tension in the conical annulus with that in the paraboloidal annulus.

2.2 DESIGN OF OUTER RIM MASS

The radial component of the meridional edge tension at the outer rim r = D/2 of the paraboloidal membrane must be reacted by some structural member external to the membrane. A convenient means of providing such reaction in this spinning case is through the centrifugal force induced by an added rim mass.

Consider a uniform rim mass with lineal mass density $\hat{m}$ as shown in Figure 2-2. The radial equation of motion of the rim mass (assuming negligible hoop-tension effects in the rim mass) is

$$\frac{D}{2}\hat{m}\omega^2 = T\cos\alpha + N_\phi \cos\beta \tag{2-21}$$

where T is the tension in the front stays per unit circumferential length around the rim, and α and β are the angles shown in Figure 2-2. The term N_ϕ is the meridional edge tension in the paraboloidal annulus at r = D/2. From geometry, it can be shown that

$$\alpha = \tan^{-1}\left(2f - \frac{1}{8f}\right) \tag{2-22}$$

$$\beta = \tan^{-1}\left(\frac{1}{4f}\right) \tag{2-23}$$

The Z-direction equation of motion of the rim mass is

$$T\sin\alpha = N_\phi \sin\beta \tag{2-24}$$

Substituting the values of N_ϕ and ω from Eqs. (2-7) and (2-11), respectively, we can obtain by using Eqs. (2-21) and (2-24) the required tension T in the front stays as well as the required rim mass $\hat{m}$. The results are

$$T = \begin{cases} 0.657 \text{ N/m}; & f = 1/2 \\ 0.226 \text{ N/m}; & f = 1 \\ 0.103 \text{ N/m}; & f = 2 \end{cases} \tag{2-25}$$

and

$$\left(\frac{\text{Mass}}{\pi D^2/4}\right)_{\text{rim mass}} = \begin{cases} 0.298 \text{ g/m}^2; & f = 1/2 \\ 0.200 \text{ g/m}^2; & f = 1 \\ 0.181 \text{ g/m}^2; & f = 2 \end{cases} \tag{2-26}$$

2.3 DESIGN OF FRONT STAYS

The required tension in the front stays is given in Eq. (2-25). Assuming a stay material of Kevlar 49 with working stress $\sigma = 6.9 \times 10^8$ N/m^2 and mass density $\rho = 1380$ kg/m^3, and assuming a uniform stay distribution of 90 stays around the circumference of the reflector rim, we performed an analysis of stay resonant frequencies and tension changes due to spinning. It was found that the stay resonant frequencies are about 5 to 20 times higher than the spin rate ω. Furthermore, it was found that the change in stay tension induced by the spin of the satellite was less than 1 percent in all cases. Hence, it is concluded that neither of these effects has a significant influence on the design.

The total mass of front stay tapes is independent of the number of tapes and is given by

$$\left(\frac{\text{Mass}}{\pi D^2/4}\right)_{\text{front stays}} = \frac{2\rho T}{\sigma \cos \alpha} = \begin{cases} 0.00329 \text{ g/m}^2; & f = 1/2 \\ 0.00192 \text{ g/m}^2; & f = 1 \\ 0.00167 \text{ g/m}^2; & f = 2 \end{cases} \tag{2-27}$$

2.4 DESIGN OF BACK STAYS

The required tension in the back stays is 2.5 N/m, as previously discussed. Since these stays are much shorter and more heavily loaded than the front stays, the potential problems induced by satellite spin (e.g., forced resonance of stay tapes and change in static tension) are even less likely to be important for the back stays than for the front. Hence, no additional consideration is required.

The mass of the back stays is given by

$$\left(\frac{\text{Mass}}{\pi D^2/4}\right)_{\text{back stays}} = \frac{4\rho T\left(\frac{H + \ell}{D}\right)}{\sigma \cos \gamma} \tag{2-28}$$

where γ, H, and ℓ are shown in Figure 2-2. From geometry, it can be shown that

$$\gamma = \begin{cases} 74.5 \text{ degrees}; & f = 1/2 \\ 82.2 \text{ degrees}; & f = 1 \\ 86.1 \text{ degrees}; & f = 2 \end{cases} \tag{2-29}$$

and

$$\left(\frac{H + \ell}{D}\right) = \begin{cases} 0.0554; & f = 1/2 \\ 0.0276; & f = 1 \\ 0.0138; & f = 2 \end{cases} \tag{2-30}$$

Assuming the back stays are made of Kevlar 49 with the same properties as those used in the design of the front stays we obtain

$$\left(\frac{\text{Mass}}{\pi D^2/4}\right)_{\text{back stays}} = \begin{cases} 0.00417 \text{ g/m}^2; & f = 1/2 \\ 0.00404 \text{ g/m}^2; & f = 1 \\ 0.00401 \text{ g/m}^2; & f = 2 \end{cases} \tag{2-31}$$

2.5 DESIGN OF INFLATED CYLINDRICAL CENTER COLUMN

One of the two structural concepts for carrying the compression load in the center column is based on the use of an inflated cylindrical tube. The tube is made of fiber-reinforced mylar with fixed gauge thickness of $t = 2.45 \times 10^{-6}$ m (0.1 mil), and the internal pressure is adjusted to carry the compressive load without benefit of compressive stress in the tube walls. Buckling strength is provided by bending stiffness in the elastic tube walls. A schematic diagram of this column is shown in Figure 2-3.

Because the column must spin with the membrane reflector, column failure may occur by whirl instability as well as buckling. To account for this fact, the design criteria for the column are based on the formula

$$(F.S.) \times \left(P + \frac{\omega^2 ML}{\pi^2} \right) = P_{cr} \tag{2-32}$$

where

$$P_{cr} = \frac{\pi^3 E r^3 t}{L^2} \tag{2-33}$$

is the Euler buckling load, and where

$$M = 2\pi rtL\rho + P\left(\frac{M_0}{R_0 T}\right) L \tag{2-34}$$

is the total mass of the column (exclusive of the end caps). The notation used here is as follows:.

F.S. = factor of safety
P = compressive end load
ω = satellite spin rate
E = modulus of elasticity of the tube wall
t = wall thickness
r = tube radius
L = column length
ρ = mass density of the tube wall

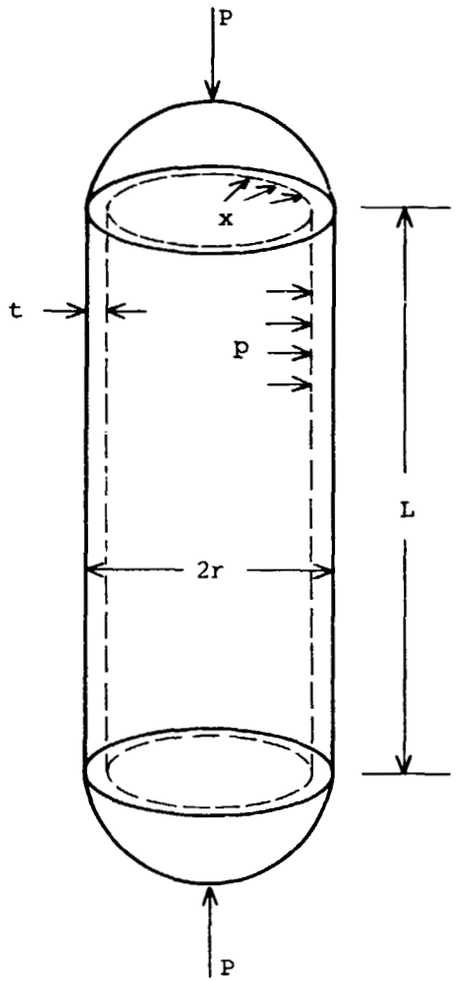

Figure 2-3. Inflated cylindrical center column. 105A

M_0 = molecular weight of pressurant

R_0 = universal gas constant

T = pressurant temperature

Local buckling of the tube wall is prevented by choosing the pressure to be

$$p = \frac{F}{\pi r^2} \tag{2-35}$$

Analysis of the whirl instability of the column yields the following result for the critical spin rate ω_{cr} of the column

$$\omega_{cr} = \frac{\pi}{L}\sqrt{\frac{P_{cr}L}{M}} \tag{2-36}$$

From a design point of view, Eqs. (2-32) through (2-34) may be regarded as an equivalent to a single cubic equation which determines the required column radius r for given gauge thickness t and other parameters. Shown in Table 2-1 are the results of this design procedure based on the column loads presented in Eqs. (2-6) and spin rates presented in Eq. (2-11). The results are based on a factor of safety of two and fiber-reinforced mylar properties of

$$E = 28 \times 10^9 \text{ N/m}^2 \tag{2-37}$$

$$\rho = 2080 \text{ kg/m}^3$$

The pressurant is assumed to be N_2 at 300 K, for which

$$\frac{M_0}{R_0 T} = 1.123 \times 10^{-5} \text{ kg/N-m} \tag{2-38}$$

In reviewing the results presented in Table 2-1, it is observed that large aperture (small F/D) designs are governed primarily by Euler buckling, while small aperture (large F/D) designs are giverned primarily by whirl instability. The relative column diameter and unit mass increase substantially with increasing (F/D), while the internal pressure simultaneously decreases. In general, the column appears to be quite

TABLE 2-1. INFLATED CYLINDRICAL CENTER COLUMN DESIGNS*
(fixed gauge thickness t = 2.45×10^{-6} m
(0.1 mil)).

(F/D)	(L/D)	(r/D)	P/D (N/m)	P_{cr}/D (N/m)	ωD (m/s)	$\omega_{cr} D$ (m/s)	pD (N/m)	$M/(\pi D^2/4)$ (g/m^2)
1/2	0.535	7.36×10^{-3}	1.23	2.96	188	640	7230	0.169
1	1.02	1.30×10^{-2}	0.625	4.49	190	317	1180	0.550
2	2.01	4.30×10^{-2}	0.315	41.9	191	272	54.2	3.53

*Material parameters: $E = 28 \times 10^9$ N/m^2, $\rho = 2080$ kg/m^3
Pressurant: N_2 at 300 K

lightweight in comparison with the membrane reflector so that a relatively balanced design is possible. Note, however, that the column radius becomes quite large for the F/D = 2 case so that the condition of Eq. (2-20) is violated. It would be necessary in this case to enlarge the inner radius r in the conical membrane to accommodate the large column which results from Table 2-1. The amount of enlargement required is not excessive, though, and the effect on the tension N_ϕ in the membrane would be beneficial in that it would be reduced from the nominal value of 35 N/m.

In closing, it should be noted that attempts were made to create alternative center column designs based on inflated isotensoid column technology (Ref. 2-2). These attempts were not considered successful in that the resulting designs were not capable (with reasonable slenderness) of satisfying the whirl stability criterion.

2.6 DESIGN OF TRUSS CENTER COLUMN

An alternative structural concept for the center column is based on the truss configuration. The truss is considered to be a coilable lattice column of typical Astromast design (Ref. 2-3). The three continuous longerons are made of a graphite-epoxy composite material, and the cross section is assumed to have the shape of an equilateral triangle. Shear stiffness is provided by diagonal tension cords, and stability of cross-sectional shape is provided by three equal-length battens which attach to the longerons in the plane of the cross section at periodic intervals, or bays, as shown in Figures 2-4 and 2-5.

Three different approaches to the design of the truss column are presented. The first approach is the most realistic, in that both local and overall imperfections are taken into account in an accurate manner. The resulting unit mass for the column is found to be unacceptably large in comparison with the membrane reflector mass in all cases except the smallest diameter, largest aperture configuration. As a result, two more design approaches are presented in order to explore the extent to which the excessive column mass may be due to imperfection effects (which were not considered in the previous design of an inflated cylindrical center column). Design of a perfect truss column under the same criteria but without imperfections yielded very little reduction in unit mass, however, indicating that the large unit

S-3 ASTROMAST INSTRUMENT BOOM
built for the AIR FORCE by ASTRO RESEARCH CORP.

Figure 2-4.

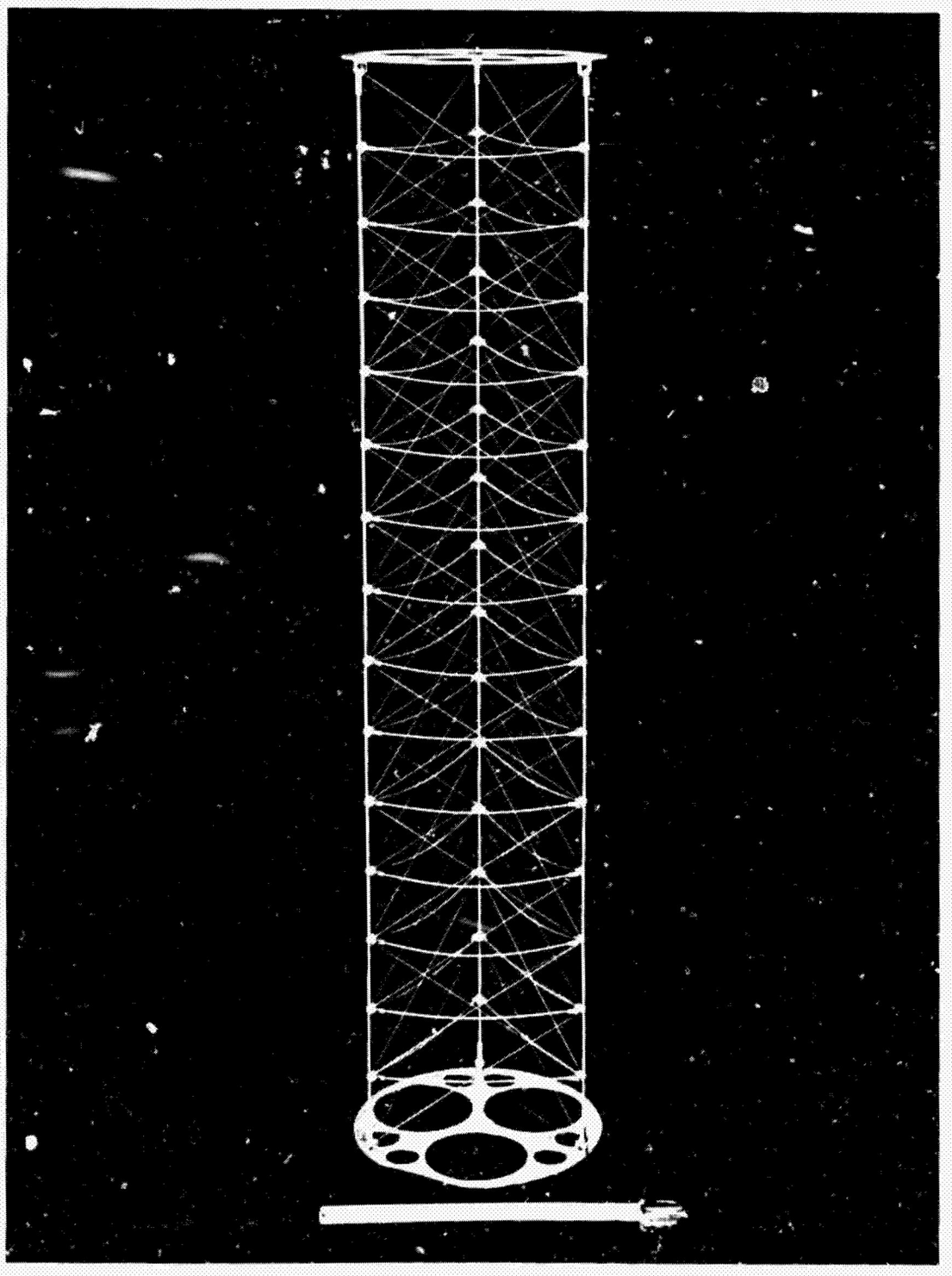

Figure 2-5.
12-inch Astromast with round longerons and dual fiberglass diagonals and battens.

mass of the truss column is not due to imperfection effects. Finally, a minimum weight design in which Euler and local buckling loads are set equal by relaxing a packaging constraint on longeron radius is employed, and substantial reduction in column unit mass is obtained. However, even in this case, the unit masses are still nearly an order of magnitude larger than those obtained for the inflated cylindrical column design.

2.6.1 Design of a Truss Column Including Effects of Initial Imperfections

Consider an Astromast truss column with both local and overall imperfections, as described in Reference 2-4. Let the local imperfection be measured by the midspan deflection amplitude δ of one bay length of longeron, and let r_g be the radius of gyration of the cross-sectional area of the longeron. Then, the local imperfections are assumed to be

$$\frac{\delta}{r_g} = \sqrt{0.1} \cong 0.316 \tag{2-39}$$

Furthermore, let the overall imperfections be measured by the midspan deflection amplitude Δ of the entire column, and note that the radius of gyration R_g of the cross-sectional area of the entire column is $R/\sqrt{2}$, where R is the radius of the column. The overall imperfection amplitude is then regarded as dependent upon the overall column slenderness ratio where

$$\beta = \frac{R}{L} \tag{2-40}$$

and L is the overall column length. In particular, let

$$\frac{\Delta}{R_g} = \begin{cases} 4.72 \times 10^{-6}\beta^{-2}; & \beta < 0.017 \\ 3.58 \times 10^{-5}\beta^{-3/2}; & \beta \geq 0.017 \end{cases} \tag{2-41}$$

This choice of Δ reflects two separate concerns, and Δ is chosen as the worst case of the two considered sources. First, for $\beta < 0.017$, Eq. (2-41) reflects midspan deflection due to an assumed variation of the coefficient of thermal expansion of $\Delta\alpha_T = 0.1 \times 10^{-6}$/K in longeron material, combined with an assumed

temperature change of $\Delta T = 100$ K with the column oriented in a worst-case direction. The longerons are assumed to have length L with $\Delta = 0$ at the reference temperature. Then, after the temperature change ΔT, one longeron is assumed to have expanded more than the other two, and the overall column length is assumed to be the average of the final lengths of all three longerons. The Δ is then calculated as the midspan deflection of the resulting circular arc shape of the overall column.

The case when $\beta \geq 0.017$ in Eq. (2-41) is based on an analysis of expected rms surface deflections in a simply supported planar truss made of straight members with imperfect initial lengths. The analysis, presented in Reference 2-5, is used where it is assumed that the standard deviation of errors in member lengths (σ_ε) is 10^{-5}, and (ℓ/R) = 1.25 and (R/H) = (2/3). The resulting rms deflection was used to identify that parabola of midspan deflection Δ with the same rms value. The resulting value of Δ was then multiplied by a factor of three. The result of this process is reported in Eq. (2-41).

Column designs were then determined from the equation

$$\left(\frac{x^*}{\frac{1 + \hat{\delta}^2/2}{K}} - 1\right)\left(\frac{1}{\frac{1 + \sqrt{3}\Delta^*}{K}} - 1\right) = C_0 + C_1 x^* \qquad (2\text{-}42)$$

where

$$K = \frac{P_b}{P_\ell} \; ; \quad \hat{\delta} = \frac{\delta}{r_g} \; ; \quad \Delta^* = \frac{\Delta/R_g}{1 - 7.55 \times 10^{-10} \omega^2 L^2 \beta^{-2}} \qquad (2\text{-}43)$$

$$x^* = \frac{P_E}{P_\ell}\left(1 - 7.55 \times 10^{-10} \omega^2 L^2 \beta^{-2}\right) \qquad (2\text{-}44)$$

where

P_b = column buckling load

P_ℓ = local buckling load of one bay length of column

P_E = Euler buckling load of overall length of column

ω = satellite spin rate (radians/second)

C_0, C_1 = empirical constants determined from detailed imperfection analysis

Equation (2-42) was determined as a simplified empirical fit to the numerical-quadrature-determined results presented in Reference 2-6 for the effects of combined local and overall imperfections on the buckling load of lattice columns. The effects of satellite spin are included in the parameters x^* and Δ^*, which reduce to static (nonspinning) values when $\omega = 0$. These spin corrections were determined from the analysis presented in Reference 2-4 by including an additional inertia load term in the governing nonlinear differential equations and then redefining the effective P_E and Δ in the Ritz solution so as to absorb the additional spin-dependent terms.

By careful examination and curve fitting of the data presented in Reference 2-6 for the buckling loads in the case where $\delta/r_g = 0.3$, the constants C_0 and C_1 are assumed as

$$C_0 = 1.4\sqrt{\Delta^*} + 0.14$$
$$C_1 = 0.135\,\Delta^* + 0.275 \qquad (2\text{-}45)$$

Equation (2-43) may be used to estimate the buckling load P_0 of a lattice column with combined local and overall imperfections while spinning with angular velocity ω. The column is then designed by requiring

$$(F.S)\ P = P_b \qquad (2\text{-}46)$$

where F.S. = Factor of Safety = 2 in this design, and P is compression load in the column.

Equations (2-41) through (2-46) provide a set of simultaneous nonlinear algebraic equations for β, assuming that

$$\frac{r}{R} = 0.006 \qquad (2\text{-}47)$$

where r is the longeron radius. Equation (2-47) is a packaging constraint which avoids longeron damage due to excessive strain in the stowed configuration. It is further assumed that

$$\frac{\ell}{R} = 1.25 \tag{2-48}$$

where ℓ is the length of one bay along the column length. Let the longeron material be graphite/epoxy composite with

$$\begin{aligned} E &= 1.245 \times 10^{11} \text{ N/m}^2 \\ \rho &= 1520 \text{ kg/m}^3 \end{aligned} \tag{2-49}$$

Presented in Table 2-2 are the resulting design parameters for a truss column with combined local and overall imperfections. Note that the column masses are much larger than those presented in Table 2-1 for the inflated cylindrical column.

2.6.2 Design of a Perfect Truss Column

In this section we investigate the extent to which the excessive column masses obtained in the preceding section for an imperfect column may have been caused by the effects of imperfections. In this design, it is again assumed that

$$\left(\frac{r}{R}\right) = 0.006 \; ; \quad \left(\frac{\ell}{R}\right) = 1.25 \tag{2-50}$$

However, the buckling strength of the column is determined by

$$P_b = \text{Minimum } (P_E^*, P_\ell) \tag{2-51}$$

where

$$P_E^* = P_E\left(1 - \frac{\omega^2 m L^2/\pi^2}{P_E}\right) \tag{2-52}$$

TABLE 2-2. IMPERFECT TRUSS COLUMN DESIGNS*
(proportional longeron radius,
r/R = 0.006)

(F/D)	ω (rad/s)	D (m)	L (m)	R (m)	P (N)	P_E (N)	P_ℓ (N)	Δ*	$M/(\pi D^2/4)$ (g/m^2)
1/2	1.88	100	53.5	0.397	123	1809	378	0.099	1.67
1/2	0.188	1,000	535	2.05	1,230	12,700	10,000	0.674	4.43
1/2	0.0188	10,000	5,350	15.8	12,300	456,000	601,000	4.25	26.4
1	1.90	100	102	0.581	62.5	2,280	812	1.15	6.80
1	0.190	1,000	1,020	5.46	625	178,000	71,400	9.19	59.9
1	0.0190	10,000	10,200	54.2	6,250	17.3×10^6	7.1×10^6	66.2	590
2	1.91	100	201	2.12	31.5	105,000	10,800	24.0	179
2	0.191	1,000	2,010	21.2	315	10.4×10^6	1.08×10^6	168	1,780
2	.0191	10,000	20,100	212	3,150	1.04×10^9	108×10^6	1,135	17,600

*Material parameters: $E = 1.245 \times 10^{11}$ N/m^2, $\rho = 1520$ kg/m^3, F.S. = 2, $\ell/R = 1.25$

where P_b, P_E, and P_ℓ are as defined in the preceding section, and m is the mass per unit length of the column. The effects of satellite spin rate are included in the effective P_E^* of Eq. (2-52), as previously discussed.

The column design is then determined from the requirement that

$$(F.S.)\ P = P_b \tag{2-53}$$

where (F.S.) = Factor of Safety = 2. Using the same material properties as those considered in the preceding section, we obtained the column designs presented in Table 2-3. Note that while the masses of the resulting perfect columns are slightly smaller than those of the corresponding imperfect columns of Table 2-2, the masses are still excessive in comparison with the inflated columns. Note also that in every case except one the design is governed by P_E^*, and the excessive masses are therefore caused by the inertia effects of satellite spin rate.

2.6.3 Design of a Minimum Weight, Perfect Truss Column

Presented in this section are the results of an investigation of the effects of relieving the constraint that r/R = 0.006. Instead, designs are determined according to the minimum weight condition that

$$P_E^* = P_\ell \tag{2-54}$$

where P_E^* is given by Eq. (2-52). In this case, r/R is regarded as an independent variable. However, Eq. (2-54) determines r/R in terms of β, ω, L, etc. The column design condition is then

$$(F.S.)\ P = P_\ell \tag{2-55}$$

where, again, F.S. = Factor of Safety = 2.

Table 2-4 presents the results of this design procedure, where it is observed that $r/R \leq 0.006$ in all but one case so that the packaging requirement is satisfied for all but one of these designs. Furthermore, a substantial savings in total column mass is realized, especially for the shallow reflector designs where (F/D) = 2.

TABLE 2-3. PERFECT TRUSS COLUMN DESIGNS*
(proportional longeron radius,
r/R = 0.006)

(F/D)	ω (rad/s)	D (m)	L (m)	R (m)	P (N)	P_E (N)	P_ℓ (N)	$M/(\pi D^2/4)$ (g/m^2)
1/2	1.88	100	53.5	0.321	123	767	246	1.09
1/2	0.188	1,000	535	1.80	1,230	7,600	7,760	3.42
1/2	0.0188	10,000	5,350	15.3	12,300	395,000	560,000	24.6
1	1.90	100	102	0.561	62.5	1,980	756	6.34
1	0.190	1,000	1,020	5.43	625	174,000	70,800	59.3
1	0.0190	10,000	10,200	54.1	6,250	17.2×10^6	7.03×10^6	589
2	1.91	100	201	2.12	31.5	104,000	10,800	179
2	0.191	1,000	2,010	21.2	315	10.4×10^6	1.08×10^6	1,780
2	0.0191	10,000	20,100	212	3,150	1.04×10^9	108×10^6	17,800

*Material parameters: $E = 1.245 \times 10^{11}$ N/m^2, $\rho = 1520$ kg/m^3, F.S. = 2, $\ell/R = 1.25$

TABLE 2-4. MINIMUM WEIGHT PERFECT TRUSS COLUMN DESIGNS*
(variable longeron radius r/R)

(F/D)	ω (rad/s)	D (m)	L (m)	R (m)	(r/R)	P (N)	P_E (N)	P_ℓ (N)	$M/(\pi D^2/4)$ (g/m^2)
1/2	1.88	100	53.5	0.252	0.00676	123	374	246	0.850
1/2	0.188	1,000	535	1.97	0.00430	1,230	5,620	2,460	2.10
1/2	0.0188	10,000	5,350	16.8	0.00262	12,300	110,000	24,600	5.65
1	1.90	100	102	0.585	0.00375	62.5	914	125	2.68
1	0.190	1,000	1,020	5.55	0.00216	625	24,800	1,250	8.02
1	0.0190	10,000	10,200	54.6	0.00123	6,250	749,000	12,500	24.9
2	1.91	100	201	2.13	0.00166	31.5	8,070	63.0	13.6
2	0.191	1,000	2,010	21.2	9.33×10^{-4}	315	251,000	630	42.9
2	0.0191	10,000	20,100	212	5.25×10^{-4}	3,150	7.93×10^{6}	6,300	135

*Material parameters: $E = 1.245 \times 10^{11}$ N/m^2, $\rho = 1520$ kg/m^3, F.S. = 2, $\ell/R = 1.25$

2.7 EFFECTS OF AN ATTITUDE CONTROL SYSTEM ON COLUMN DESIGN

One of the special problems associated with a spin-stiffened satellite is that of overcoming the large angular momentum during attitude control maneuvers. One approach to this problem is to add a large counter-rotating flywheel to nullify the angular momentum of the reflector and obtain an overall configuration with zero net angular momentum. The added flywheel might naturally be positioned on the central compression column behind the reflector, as shown in Figure 2-6.

In this configuration, the flywheel-reflector pair might behave as a pair of control-moment gyroscopes (CMG) for efficiently providing attitude control and maneuvers of the entire satellite. The required large flywheel could be deployable and made in an isotensoid configuration of high strength fibers, as described in Reference 2-7. However, the intent here is not to explore the details of the design of such a control system, but rather to explore the effects such a system might have on the central compression column.

For a certain useful range of design parameters, a large flywheel control system might have the local effect of "clamping" the base of the central column as if cantilevered from a fixed point in space. The fundamental vibration mode of the overall spacecraft in this case might resemble that of a cantilever beam-column (representing the flexural behavior of the stiff central column) with an added tip mass (representing the rocking behavior of the spinning reflector in the rigid body mode), as shown schematically in Figure 2-7.

An analysis of the system shown in Figure 2-7 with parameters chosen to fit the inflated cylindrical column designs of Section 2.5 reveal that the combined effects of the tip mass and relaxed (cantilevered) boundary conditions lower the fundamental vibrational frequency well below the satellite spin rate ω. The results of the analysis are shown in Table 2-5. It is thus concluded that none of the inflated column designs presented in Section 2.5 is sufficiently stiff to avoid whirl instability in a direct way.

A single-term approximation to the fundamental frequency of the system shown in Figure 2-7 is given by

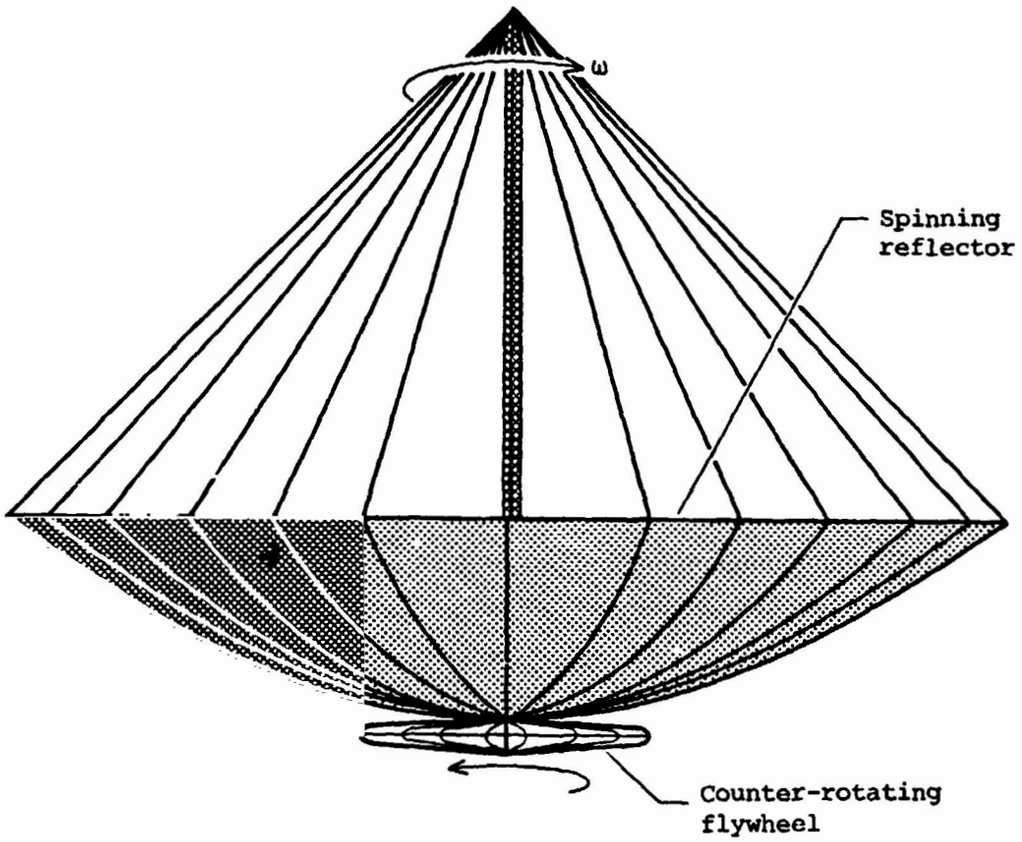

Figure 2-6. Counter-rotating flywheel attitude control system for spinning reflector spacecraft.

106A

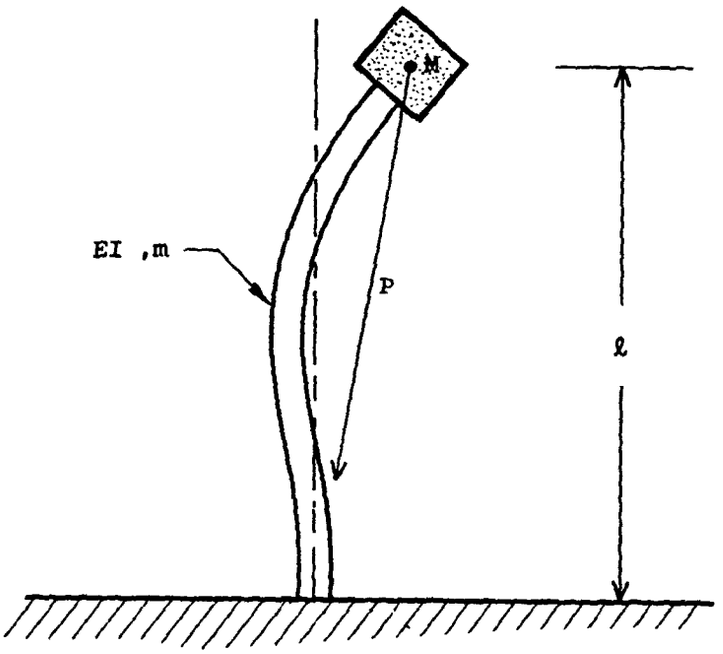

Figure 2-7. Cantilevered beam-column with tip mass model for fundamental vibration frequency of satellite in Figure 2-6. *107A*

TABLE 2-5. COMPARISON OF SATELLITE FUNDAMENTAL FREQUENCY AND SPIN RATE FOR CMG-CONTROLLED SPACECRAFT (inflated cylindrical column designs of Table 2-1).

(F/D)	I/D^3 (m)	(L/D)	$\rho AL/D^2$ (g/m^2)	M/D^2 (g/m^2)	ωD (m/s)	$\omega_n D$ (m/s)	$\omega_1 D$ (m/s)	$\omega_2 D$ (m/s)
1/2	3.07×10^{-12}	0.535	0.133	0.919	188	42.1	230	641
1	1.69×10^{-11}	1.02	0.432	0.205	190	65.8	114	317
2	6.12×10^{-10}	2.01	2.77	0.0496	191	94.1	97.6	272

Key: I = Area moment of inertia of column cross section
ρAL = Column mass; M = tip mass; ω = spin rate
ω_n = Cantilevered natural frequency (Figure 2-7)
ω_1 = Cantilevered natural frequency with M = 0
ω_2 = Simply supported natural frequency
L = Column length; D = satellite diameter

$$\omega_n = \sqrt{\frac{\frac{3EI}{\ell^3} - 0.2\,\frac{P}{\ell}}{M + 0.236\ m\ell}} \qquad (2\text{-}56)$$

Solving Eq. (2-56) for EI, replacing ω_n with the spin rate ω, and including a safety factor, we obtain the following design requirement for the central column

$$EI = (F.S.)\ x \left[\frac{w^2\ell^3}{3}\ (M + 0.236\ m\ell) + \frac{P\ell^2}{15}\right] \qquad (2\text{-}57)$$

Considering the inflated cylindrical column with fixed gauge thickness t described in Section 2.5, and using the same material properties and pressurant conditions with a F.S. = 2, we used Eq. (2-57) to determine design parameters for an inflated cylindrical center column which is consistent with attitude control philosophy previously described. The results of this design procedure are presented in Table 2-6. Comparing the column masses presented in Tables 2-1 and 2-6, we can see that it is apparent that the control approach shown in Figure 2-6 results in an approximate three-fold increase in the column mass.

The effects of alternative attitude control schemes were not examined.

2.8 SATELLITE MASS MOMENT OF INERTIA RATIOS

Another of the special problems encountered in a spin-stiffened satellite is that of the dynamic stability of the free flying spinning vehicle. It is well known that a free flying spinning vehicle is stable only when spinning about the principal axis of inertia associated with the largest mass moment of inertia. Since the subject spacecraft is intended to spin in a stable manner about an axis through the center column, an evaluation of the moment of inertia about this axis I_s (the spin axis) and also about an axis orthogonal to the column but through the mass center I_t (the tumble axis) was performed. The spinning spacecraft is then stable if I_s is greater than I_t and unstable otherwise. The results of the calculation are presented in Table 2-7.

TABLE 2-6. DESIGNS FOR INFLATED CYLINDRICAL COLUMN IN ATTITUDE-CONTROLLED SPACECRAFT (fixed gauge thickness, $t = 2.45 \times 10^{-6}$ m (0.1 mil)).

(F/D)	(L/D)	(r/D)	P/D (N/m)	P_{cr}/D (m/s)	ωD (m/s)	$\omega_{cr} D$ (m/s)	pD (N/m)	$M/(\pi D^2/4)$ (g/m^2)
1/2	0.535	0.0259	1.23	129	188	267	584	0.574
1	1.02	0.0393	0.625	124	190	269	129	1.64
2	2.01	0.120	0.315	901	191	270	7.02	9.80

*I_s = spin axis inertia, I_t = tumble axis inertia

TABLE 2-7. MASS MOMENT OF INERTIA RATIOS FOR SPINNING PARABOLOIDAL REFLECTOR SPACECRAFT*

(F/D)	(I_s/I_t)
1/2	1.74
1	0.916
2	0.167

*I_s = spin axis inertia

I_t = tumble axis inertia

Column designs taken from Table 2-6.

Clearly, the cases where (F/D) = 1 and 2 require additional mass around the outer rim of the reflector to provide dynamic stability of the spinning spacecraft. No calculation of the magnitude of the required mass was performed.

REFERENCES

2-1. Robbins, W.M., Jr.: Spinning Paraboloidal Tension Networks. NASA CR-873, 1967.

2-2. Hedgepeth, J.M.; and Miller, R.K.: Final Report - A Study of Structural Concepts for Ultralightweight Spacecraft. Astro Research Corporation, ARC-TN-1114, 14 July 1982.

2-3. Astromast for Space Applications. Astro Research Corporation, ARC-TN-004, 1983.

2-4. Miller, R.K.; and Hedgepeth, J.M.: The Buckling of Lattice Columns with Stochastic Imperfections. Int. J. Solids Structures, vol. 15, pp. 73-84, 1979.

2-5. Hedgepeth, J.M.: Accuracy Potentials for Large Space Antenna Reflectors with Passive Structure. J. Spacecraft, vol. 19, No. 3, pp. 211-217, May-June 1982.

2-6. Preiswerk, P.: Imperfections and Their Effects on the Astromast Design of the High Packing Density Ultralightweight, Extensible Boom (Square Solar Sail. Astro Research Corporation, ARC-TN-1033, 11 April 1977.

2-7. Hedgepeth, J.M.; Miller, R.K.; and Knapp, K.: Conceptual Design Studies for Large Free-Flying Solar-Reflector Spacecraft. NASA CR 3438, June 1981.

SECTION 3

DESIGN OF A TRUSS-SUPPORTED PARABOLOIDAL REFLECTOR SPACECRAFT

The design procedures used to develop the dimensions and masses of spacecraft structural components for a truss-supported paraboloidal reflector spacecraft are reported in this section. Results are presented for support structures with deep truss design and also for a geodesic dome/stiff perimeter ring configuration. A tripod truss structure is designed to support the electronic payload located at the feed of the paraboloid in each case.

3.1 DESIGN OF A DEEP TRUSS PARABOLOIDAL REFLECTOR

Consider a deep truss in the shape of a paraboloid, as shown in Figure 3-1. The truss has nominal depth H, and the reflective surface is composed of nominally equilateral triangular facets of length ℓ, as shown in the figure. A reflective mesh or membrane is stretched and supported along the upper surface of the truss, while the lower surface does not support a mesh. The interface between the mesh and truss occurs only at the triangular lattice nodes. Separate tendons under high tension are laced through the mesh along lines parallel to the surface truss elements and attached at the nodes. The truss members therefore must carry only axial compression and tension and can thus be slender for lightly loaded situations. Properly located joints allow stowage and deployment of the otherwise uncompliant structure. From an overall standpoint, the tetrahedral truss structure can be thought of as a thick shell, the surface of which is defined by the lattice nodes. For the equilateral triangular geometry shown, the shell is isotropic, an advantage that does not obtain for some other truss geometries.

Let the edge tension in the mesh be isotropic with a unit value of N Newtons per meter. Then, assuming a tenfold amplification of tension loads in the tendons, we obtain the induced compression in a typical truss member near the perimeter of the truss

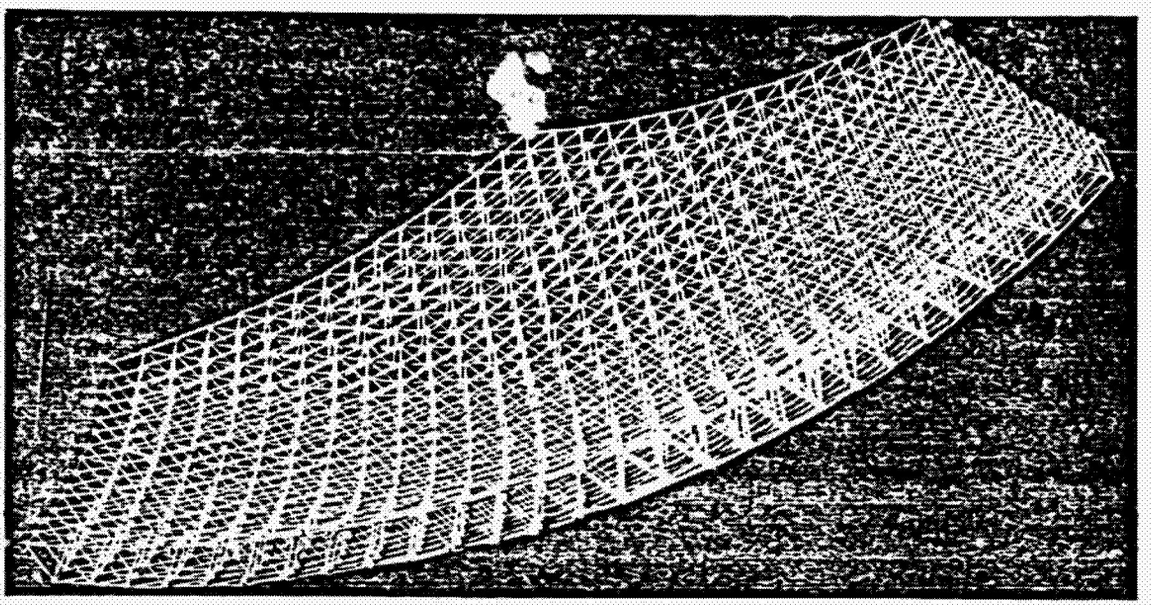

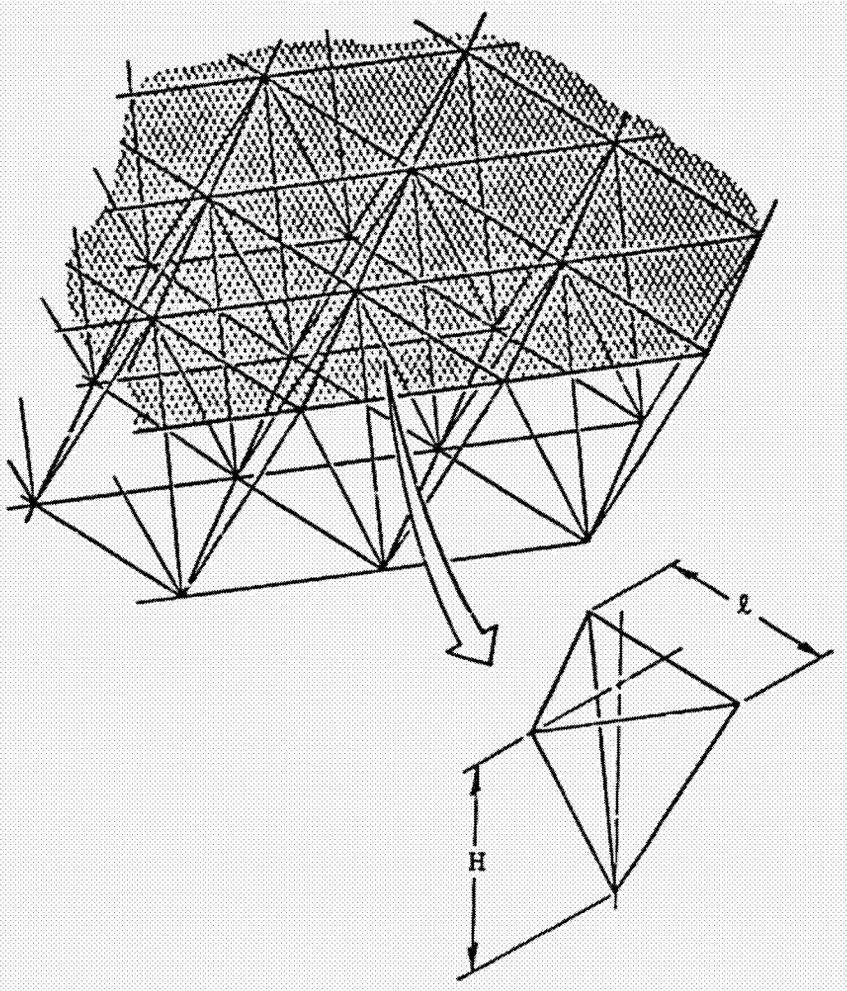

Figure 3-1. Tetrahedral truss configuration.

$$P = \frac{10\,N\ell}{\sqrt{3}} \tag{3-1}$$

Furthermore, let each truss member be a thin-walled hollow tube with wall thickness t and designed to carry the compression load P as an Euler column with a factor of safety of F.S. Then, as shown in Reference 3-1, the resulting diameter to length ratio of the member is

$$\frac{d}{\ell} = \left(\frac{8\ F.S.}{\pi^3}\frac{P}{t\ell E}\right)^{1/3} \tag{3-2}$$

where E is the modulus of elasticity of the tube material.

Substituting from Eq. (3-1) into Eq. (3-2), we find the truss member slenderness ratio to be

$$\frac{d}{\ell} = \left(\frac{80\ F.S.}{\sqrt{3}\,\pi^3}\frac{N}{tE}\right)^{1/3} \tag{3-3}$$

The strut length ℓ may be determined by limiting the rms deviation between the flat mesh facets and the desired paraboloidal surface to be less than some predetermined value. Since the rms deviation decreases with ℓ, it is possible, at least in principle, to meet any arbitrarily demanding surface accuracy requirement by simply reducing ℓ sufficiently, thereby increasing the number of facets in the approximating mesh surface.

Let w_{rms} be the rms deviation just described, let D be the diameter of the reflector, and let F be the focal length of the desired paraboloid. Then, it may be shown (Ref. 3-1, p.161) that the required strut length ℓ for a given allowable rms deviation is given by

$$\frac{\ell}{D} = 7.87\sqrt{\frac{F}{D}\left(\frac{w_{rms}}{D}\right)_{allow.}} \tag{3-4}$$

For the tetrahedral truss, the total mass of the truss structure is independent of ℓ, however. In fact, it can be shown (Ref. 3-1, p. 169) that the structural mass per unit area of the tetrahedral truss is given by

$$\frac{\text{mass}}{\text{area}} = 4k\rho\sqrt{3}\left(\frac{F.S.\ Pt^2}{\ell E}\right)^{1/3}\left[2+\sqrt{\frac{1}{3}+\left(\frac{H}{\ell}\right)^2}\right] \tag{3-5}$$

where ρ is the mass density of the truss material and k is a factor to account for the mass of the fittings. In addition, the surface area A_{par} of the desired paraboloid may be related to the frontal area of the reflector as follows:

$$\left(\frac{A_{par}}{\pi D^2/4}\right) = \begin{cases} 1.06011; & F/D = 1/2 \\ 1.01547; & F/D = 1 \\ 1.00390; & F/D = 2 \end{cases} \tag{3-6}$$

Assuming a graphite/epoxy material for the truss members with

$$E = 1.0 \times 10^{11}\ N/m^2; \quad \rho = 1520\ kg/m^3 \tag{3-7}$$

and a fixed wall thickness of

$$t = 0.35\ mm \tag{3-8}$$

also a factor of safety of

$$F.S. = 2 \tag{3-9}$$

a fittings mass factor of

$$k = 1.5 \tag{3-10}$$

and an allowable rms surface error of

$$\left(\frac{w_{rms}}{D}\right)_{allow.} = 10^{-5} \tag{3-11}$$

we may obtain the structural mass per unit area for tetrahedral truss designs given in Table 3-1. The truss depth H used in these designs is equal to the surface member length ℓ.

3.1.1 Slenderness Requirements on Truss Members

The proposed truss member designs given in Table 3-1 were evaluated with respect to the slenderness requirements suggested in Reference 3-2. These requirements ensure that certain fabrication, testing, and assembly processes may be accomplished without seriously degrading the properties of the truss.

For a thin-walled tube, the radius of gyration r_g of the cross section is related to the tube radius r by

$$r_g = \frac{r}{\sqrt{2}} = \frac{d}{2\sqrt{2}} \tag{3-12}$$

Thus, the parameter of interest in Reference 3-2 is

$$\frac{\ell}{r_g} = \frac{2\sqrt{2}\ell}{d} \tag{3-13}$$

For all designs given in Table 3-1, it can be shown that

$$\frac{\ell}{d} = 235 \tag{3-14}$$

so that

$$\frac{\ell}{r_g} = 665 \tag{3-15}$$

3.1.2 Requirement 1 - Horizontal Testing

To accommodate standard structural testing of the truss members in the horizontal position in the Earth's gravitational field, it is shown in Reference 3-2 that the requirement on slenderness is

TABLE 3-1. PARABOLOIDAL TETRAHEDRAL TRUSS DESIGNS*
(mesh mass not included).

(F/D)	P/D (N/m)	P_{cr}/D (N/m)	ℓ/D	d/D	Mass/($\pi D^2/4$) (g/m^2)
1/2	0.102	0.204	0.0176	7.50×10^{-5}	124
1	0.144	0.288	0.0249	1.06×10^{-4}	119
2	0.203	0.406	0.0352	1.50×10^{-4}	117

*Material parameters: $E = 1.1 \times 10^{11}$ N/m^2, $\rho = 1520$ kg/m^3, $t = 0.35$ mm, F.S. = 2, $k = 1.5$, $H = \ell$, $(w_{rms}/D) = 10^{-5}$

$$\frac{\ell}{r_g} < \frac{574}{\ell^{1/3}} \tag{3-16}$$

for the materials and wall thickness used in Table 3-1. A check of the designs presented in the table for D = 100, 1,000, and 10,000 m reveals that all designs fail this requirement.

3.1.3 Requirement 2 - Vertical Testing

This requirement for standard structural testing of the truss members in the vertical position in the Earth's gravitational field is based on the criterion that tension load induced by the weight of the member should not exceed one-tenth of the Euler buckling load of the member. As shown in Reference 3-2, the corresponding requirement on slenderness is

$$\frac{\ell}{r_g} < \frac{2700}{\ell^{1/2}} \tag{3-17}$$

Evaluating the designs of Table 3-1 for this requirement, we find that designs with all three (F/D) values pass this test when D = 100 m, but all fail for D = 1,000 and 10,000 m.

3.1.4 Requirement 3 - Fabrication Tolerances

Assuming a strain variation of $\Delta\varepsilon = 10^{-6}$, we can see from Reference 3-2 that this requirement on slenderness is

$$\frac{\ell}{r_g} < 1533 \tag{3-18}$$

All designs pass this test.

3.1.5 Requirement 4 - Built-In Loads Due to Member Length Errors

Assuming a variation in member length of $\sigma_\varepsilon = 10^{-5}$, we find that the corresponding requirement that the resulting built-in member loads be smaller than one-tenth the Euler load is (Ref. 3-2)

$$\frac{\ell}{r_g} < 414 \qquad (3\text{-}19)$$

All designs fail this test, though not by an excessive margin.

3.1.6 Requirement 5 - Member Vibration Frequencies

Requiring that the truss members be sufficiently stiff that their fundamental vibration frequency be at least three times the fundamental frequency of the assembled truss, we can see from Reference 3-2 that for $m_p/m_s = 2$, $k = 2$, and $H = \ell$ the slenderness requirement is

$$\frac{\ell}{r_g} = 2260 \qquad (3\text{-}20)$$

All designs pass this test.

In summary, the proposed truss designs have adequate slenderness to provide a competent realizable structure, but testing the truss members in Earth's gravity field would likely present some special difficulties.

3.2 DESIGN OF A GEODESIC DOME PARABOLOIDAL REFLECTOR

Consider a geodesic dome in the shape of a paraboloid, as shown in Figure 3-2. The geodesic dome behaves in the large as a membrane, and it can be viewed as the limiting case of a tetrahedral truss as the thickness H is reduced to zero. It is simpler than the truss since only one surface of lattice elements is required. On the other hand, the membrane-like surface is very flexible unless the edge is supported by a stiff ring. Packaging and deploying the ring may present more difficulties than those presented by the more nearly uniform tetrahedral truss. The interface with the mesh is again assumed to be at the lattice nodes, and the structural members carry axial tension and compression only.

All strength and surface accuracy requirements presented in the previous section for the tetrahedral truss also apply to the geodesic dome. However, the unit mass of the dome structure is much lighter than the tetrahedral truss and is given by (Ref. 3-1, p. 168)

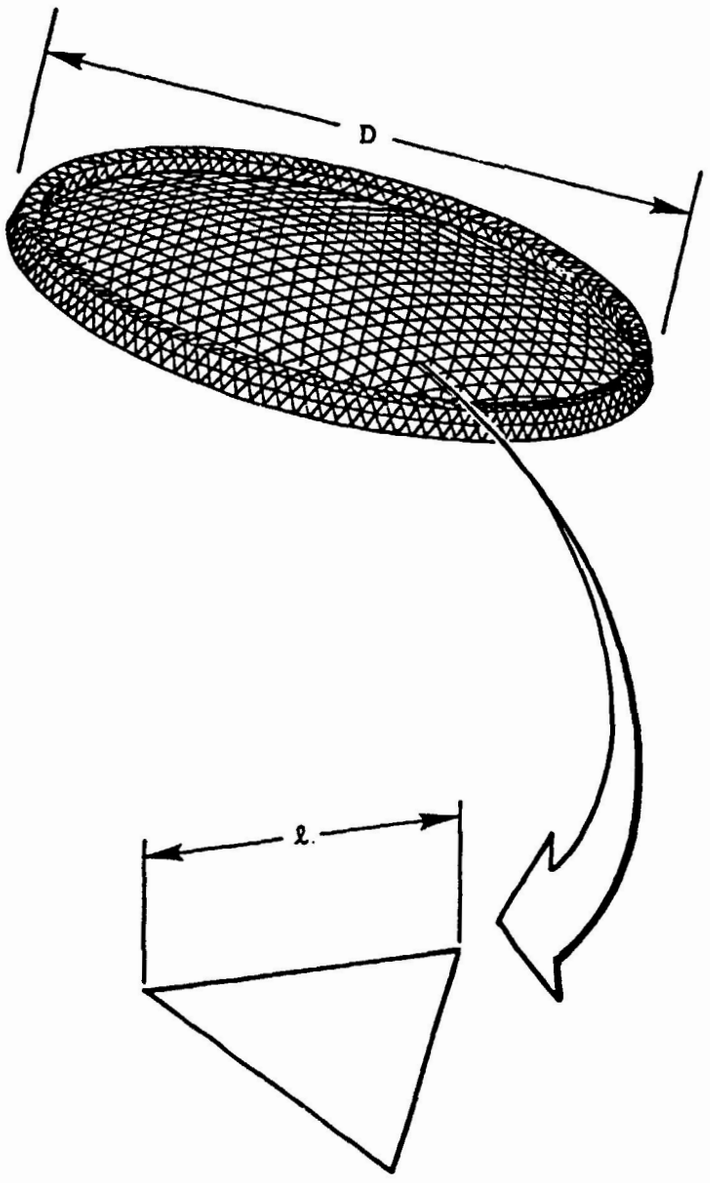

Figure 3-2. Geodesic dome configuration.

$$\frac{\text{mass}}{\text{area}} = \left(4k\rho\sqrt{3}\ \frac{\text{F.S. Pt}^2}{\ell E}\right)^{1/3} \tag{3-21}$$

Assuming all material properties, strength, and accuracy requirements for the geodesic dome are identical to those used for the tetrahedral truss designs, we obtain the results presented in Table 3-2. Although the unit masses reported in Table 3-2 for the geodesic dome are much smaller than those reported in Table 3-1 for the tetrahedral truss, the two figures are not directly comparable since the geodesic dome structure is not stiff enough to be useful until a stiff ring is added around the perimeter of the dome. Thus, the unit mass of the required ring stiffness must be added to the unit mass of the dome before a direct comparison with the tetrahedral truss can be made. The design of this ring stiffener is reported in the next section.

3.3 DESIGN OF A RING STIFFENER FOR THE GEODESIC DOME REFLECTOR

Presented in the Appendix is an analysis of the free vibrations of a shallow spherical membrane dome. In particular, the fundamental frequency of vibration of the dome with a clamped circular edge is obtained. Also obtained is the first nonzero vibration frequency of a dome whose edge is supported by a ring stiffener with isotropic bending stiffness EI. The ring stiffener is assumed to be inextensible.

The design of the ring stiffener is based on the analysis presented in the Appendix. The philosophy behind the ring design is that the ring should be stiff enough that the fundamental vibration frequency of the ring-stiffened dome is equal to the natural frequency of a dome with clamped eged. Clearly, any additional ring stiffness is not useful since it cannot further increase the natural frequency of a stiffened dome. Based on this approach, the required ring bending stiffness is given by

$$EI = \left(\frac{D}{2a}\right)^2 \left(\frac{EtD^3}{256}\right)\left(\frac{3}{2} + \frac{m_r}{m_s}\right) \tag{3-22}$$

where

TABLE 3-2. PARABOLOIDAL GEODESIC DOME DESIGNS*
(mesh mass not included).

(F/D)	P/D (N/m)	P_{cr}/D (N/m)	ℓ/D	d/D	Mass/$(\pi D^2/4)$ (g/m^2)
1/2	0.102	0.204	0.0176	7.50×10^{-5}	39.3
1	0.144	0.288	0.0249	1.06×10^{-4}	37.7
2	0.203	0.406	0.0352	1.50×10^{-4}	37.1

*Material parameters: $E = 1.1 \times 10^{11}$ N/m^2, $\rho = 1520$ kg/m^3, $t = 0.35$ mm, F.S. = 2, $k = 1.5$, $(w_{rms}/D) = 10^{-5}$

a = radius of sphere (approximately 2F)

t = effective thickness of membrane dome

E = modulus of elasticity of dome and ring

D = reflector diameter

m_r = total mass of ring

m_s = total mass of dome

The results presented in Eq. (3-22) for a spherical membrane dome may be adapted to the paraboloidal geodesic dome truss by setting

$$a = 2F \tag{3-23}$$

and by choosing an effective Et for the truss as (Ref. 3-1)

$$Et_{effective} = \frac{2}{\sqrt{3}} \frac{EA_s}{\ell} \tag{3-24}$$

where

A_s = cross-sectional area of a dome truss member

ℓ = length of a dome truss member (Figure 3-2)

Let the ring be constructed of three longerons in an equilateral triangular configuration as shown in Figure 3-3. The cross-sectional area of each longeron is assumed to be A_r, and the "radius" of the triangular stiffener cross section is R. Then it follows that the ring bending stiffness is

$$EI = \frac{3}{2} EA_r R^2 \tag{3-25}$$

The mass of the ring stiffener may be estimated as three times the mass of the longerons. Thus,

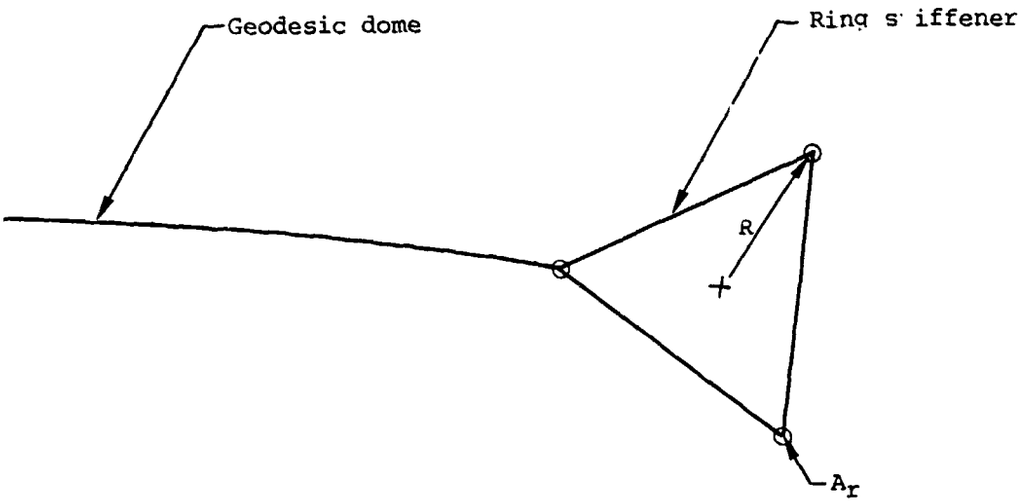

Figure 3-3. Cross-sectional view of ring stiffener and edge of geodesic dome.

111A

$$m_r = 9\pi\rho D A_r \tag{3-26}$$

The mass of the dome may be obtained from Eq. (3-21). Then Eqs. (3-21) and (3-26) give

$$\left(\frac{m}{m_s}\right) = 4\sqrt{3}\left(\frac{\ell}{D}\right)\left(\frac{A_r}{A_s}\right) \tag{3-27}$$

where the value of (ℓ/D) depends on (F/D) as given in Eq. (3-4).

Substituting from Eqs. (3-23) through (3-27) into Eq. (3-22) and using the material properties given in Eqs. (3-7), we find the relation between the required ring cross-sectional radius R and the longeron cross-sectional area A_r is

$$\left(\frac{R}{D}\right)^2 = \frac{1}{3072\sqrt{3}}\left(\frac{D}{F}\right)^2\left(\frac{D}{\ell}\right)\left(\frac{s}{A_r}\right)\left[\frac{3}{2} + 4\sqrt{3}\left(\frac{\ell}{D}\right)\left(\frac{A_r}{A_s}\right)\right] \tag{3-28}$$

Requiring in addition to Eq. (3-28) that the axial stiffness of the ring be ten times the axial stiffness of a dome truss member (in order that the ring behave in an essentially inextensional manner), we obtain the additional constraint

$$\frac{A_r}{A_s} = \frac{10}{3} \tag{3-29}$$

Finally, substituting from Eq. (3-29) into Eqs. (3-27) and (3-28), we obtain the rim mass and radius.

Presented in Table 3-3 are the resulting design characteristics for the ring stiffener. Note that in every case, the rim mass is smaller than the dome mass.

3.4 PARAMETRIC MASS RELATIONS FOR THE TETRAHEDRAL TRUSS AND GEODESIC DOME SUPPORT STRUCTURES

The equations for the unit mass of the tetrahedral truss and geodesic dome support structures, in terms of the mesh tension, are

TABLE 3-3. RING-STIFFENER DESIGNS*
(dome mass not included).

(F/D)	ℓ/D	A_r/A_s	m_r/m_s	R/D
1/2	0.0176	3.33	0.406	0.156
1	0.0249	3.33	0.575	0.0685
2	0.0352	3.33	0.813	0.0304

*Material parameters: $E = 1.1 \times 10^{11}$ N/m^2, $\rho = 1520$ kg/m^3, $k = 1.5$, $(w_{rms}/D) = 10^{-5}$

$$\frac{\text{Mass}}{(\pi D^2/4)} = 4\sqrt{3}\,\rho k K \left[\frac{(F.S.)\,t^2}{E}\,\frac{10\,N}{\sqrt{3}}\right]^{1/3}\left(2+\sqrt{\frac{4}{3}}\right) \tag{3-30}$$

for the tetrahedral truss, and

$$\frac{\text{Mass}}{(\pi D^2/4)} = \begin{cases} 4\sqrt{3}\,\rho k K\left[\dfrac{(F.S.)\,t^2}{E}\,\dfrac{10\,N}{\sqrt{3}}\right]^{1/3} & \text{(dome only)} \\ 4\sqrt{3}\,\rho k K\left[\dfrac{(F.S.)\,t^2}{E}\,\dfrac{10\,N}{\sqrt{3}}\right]^{1/3} \times \left[1+4\sqrt{3}\left(\dfrac{\ell}{D}\right)\left(\dfrac{A_r}{A_s}\right)\right] & \text{(dome + ring)} \end{cases} \tag{3-31}$$

for the dome, where

$$K = \begin{cases} 1.06011; & F/D = 1/2 \\ 1.01547; & F/D = 1 \\ 1.00390; & F/D = 2 \end{cases} \tag{3-32}$$

and where the truss loading of Eq. (3-1) has been assumed, and also $H = \ell$. As discussed in Section 3.3, the area ratio $(A_r/A_s) = 10/3$ was assumed in the design of the ring stiffener for the dome.

If the material properties, wall thickness, factor of safety, and fitting mass factor values used in Tables 3-1 and 3-2 are used, the unit mass of both structures may be regarded as dependent upon the assumed mesh tension N through the relations

$$\frac{\text{Mass}}{(\pi D^2/4)} = \begin{cases} 124\,N^{1/3}; & F/D = 1/2 \\ 119\,N^{1/3}; & F/D = 1 \\ 117\,N^{1/3}; & F/D = 2 \end{cases} \quad \text{Tetrahedral Truss} \tag{3-33}$$

$$\frac{\text{Mass}}{(\pi D^2/4)} = \begin{cases} 39.2\,N^{1/3}; & F/D = 1/2 \\ 37.6\,N^{1/3}; & F/D = 1 \\ 37.1\,N^{1/3}; & F/D = 2 \end{cases} \quad \begin{array}{l}\text{Geodesic Dome} \\ \text{(without ring)}\end{array} \tag{3-34}$$

$$\frac{\text{Mass}}{(\pi D^2/4)} = \begin{cases} 55.1\ N^{1/3}; & F/D = 1/2 \\ 59.2\ N^{1/3}; & F/D = 1 \\ 67.3\ N^{1/3}; & F/D = 2 \end{cases} \qquad \begin{matrix} \text{Geodesic Dome} \\ \text{+ Ring Stiffener} \end{matrix} \qquad (3\text{-}35)$$

where the unit mass values have units of grams per square meter when the mesh tension N is expressed in Newtons per square meter.

A plot of these unit masses vs. mesh tension is shown in Figure 3-4.

3.5 DESIGN OF A TRIPOD SUPPORT STRUCTURE FOR THE PARABOLOIDAL REFLECTOR FEED

In order to complete the truss reflector design, a tripod made of lightweight columns is required to extend from the rim of the reflector up to the focal point of the paraboloid, as shown in Figure 3-5. The three identical columns are located at points equidistant around the reflector rim, and each has length L where

$$\left(\frac{L}{D}\right) = \sqrt{1 + \left(\frac{F}{D} - \frac{D}{16F}\right)^2} \qquad (3\text{-}36)$$

where D is the diameter of the reflector rim, and F is the focal distance of the paraboloidal reflector.

Let each column of the tripod be made from three identical longerons arranged to form an equilateral triangle in cross section. Furthermore, let this triangle be sized such that the longerons will intersect the reflector truss at three adjacent joints on the reflector surface, as shown in Figure 3-6. Thus, the required batten length ℓ is the same as the length of the truss members which form the equilateral triangular facets on the reflective surface of the truss.

Also, let the column longerons be composed of equal bays of the same length ℓ. Then the column may be composed entirely of members identical to those used to form the reflective surface of the truss, except for the cross bracing necessary to provide shear strength. The cross bracing will be assumed to consist of pretensioned fibers not capable of sustaining compression and therefore will be extremely lightweight in comparison with the compression members in the column.

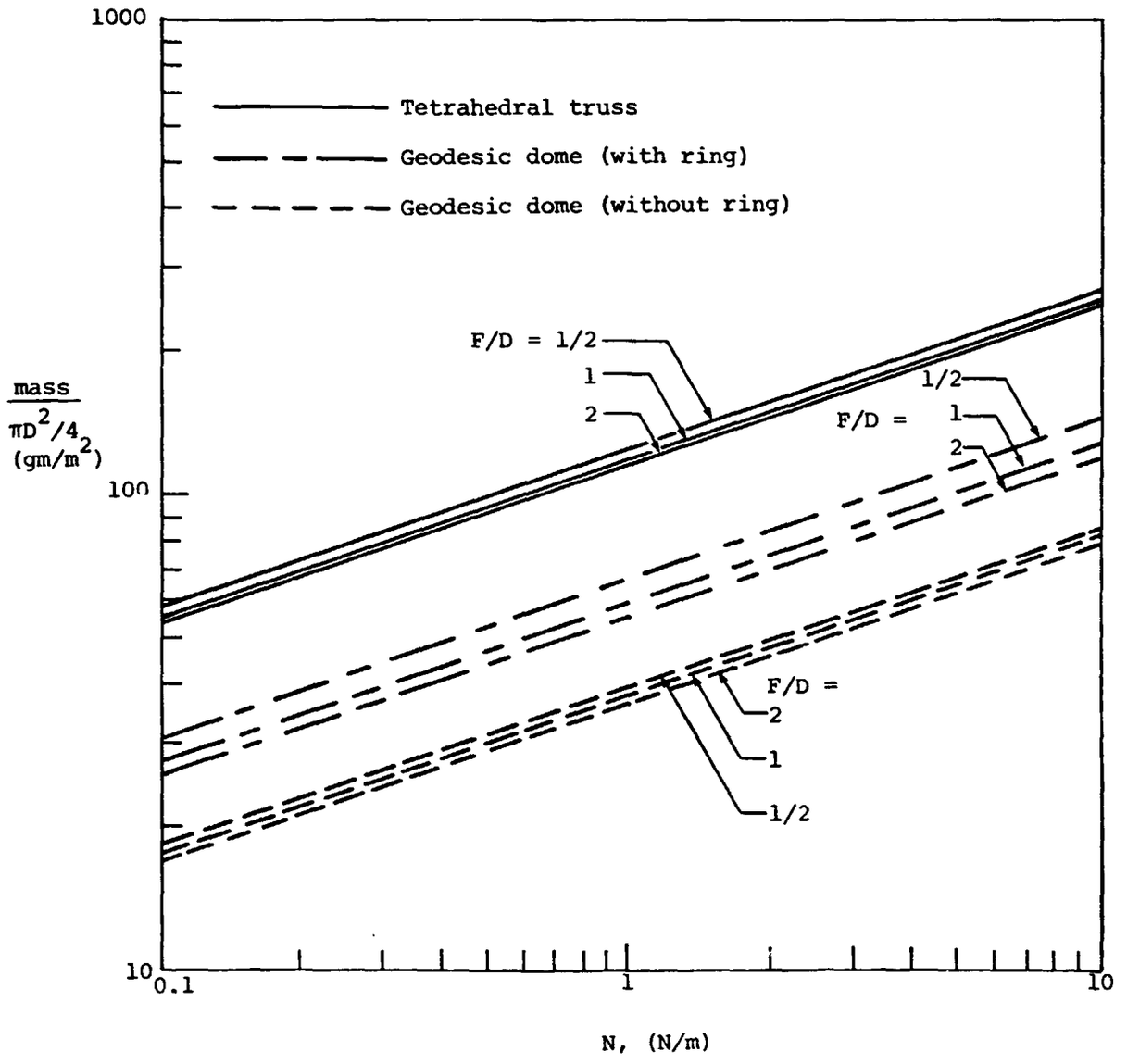

Figure 3-4. Unit mass vs. mesh tension for truss support structures (not including mesh itself), solid tube designs (t = 0.35 mm, graphite/epoxy). *108A*

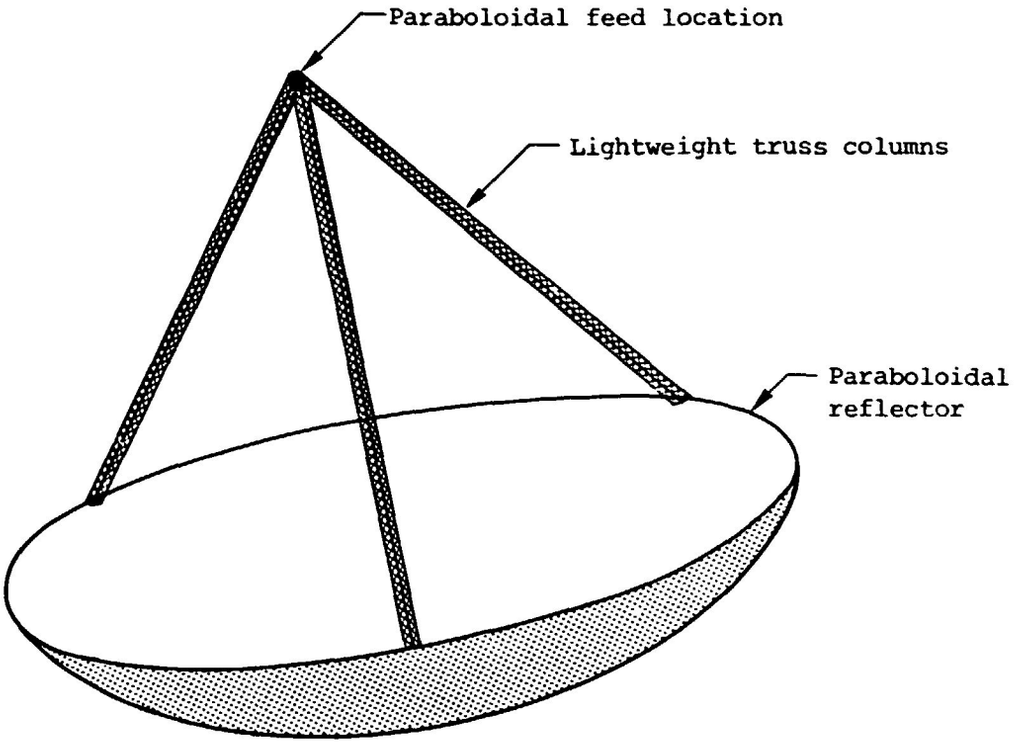

Figure 3-5. Tripod feed support structure. *110A*

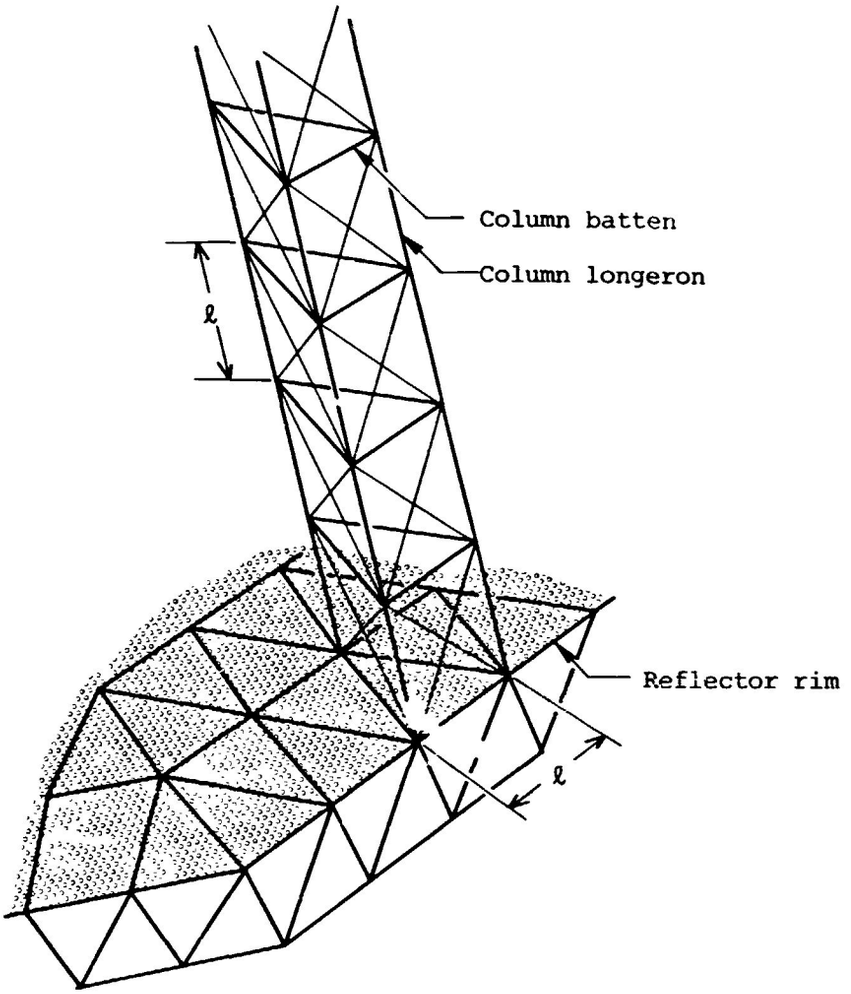

Figure 3-6. Tripod column/reflector surface interface. *109A*

Choosing column compression members with length, diameter, wall thickness, and material properties identical to those used for truss members in the reflector surface, the strength and flexibility coefficients of the resulting tripod are presented in Table 3-4. The buckling loads presented in Table 3-4 are for axially loaded individual columns, while the flexibility coefficients are for a complete tripod assembly assuming a rigid reflector.

The mass of the tripod may be determined from

$$\left(\frac{\text{Mass}}{\pi D^2/4}\right) = 144\ k\rho t \left(\frac{L}{D}\right)\left(\frac{d}{D}\right) \qquad (3\text{-}37)$$

where k is a factor intended to account for added masses from joint fittings and diagonal bracing. For the tripod masses presented in the table, k was assumed to be 2.

3.6 DESIGN OF A PARABOLOIDAL TETRAHEDRAL TRUSS REFLECTOR WITH INFLATED STRUTS

Since the total spacecraft unit mass in the tetrahedral truss configuration is quite large in comparison with available alternative configurations, an investigation of the effect on the unit mass of considering inflated truss members instead of solid tubes was performed. In this investigation, the column compression loads P and lengths ℓ were chosen from Table 3-1 to be identical to those used in the solid tube design. The inflated strut design was assumed to be a circular cylinder with fixed gauge-thickness of t = 1 mil = 2.45×10^{-5} m, and material of axial fiber-reinforced mylar skin. The pressurant was assumed to be N_2 at 300 K. The buckling strength is proportional to the modulus of elasticity of the graphite fibers, which was assumed to be 2.21×10^{11} N/m^2. The mass density of the mylar skin was taken as ρ_s = 2080 kg/m^2, while that for the fibers was ρ_f = 1750 kg/m^2. A factor of safety against Euler buckling of the struts was chosen as 2, as was the fitting mass factor.

TABLE 3-4. SUMMARY OF TRIPOD STRENGTH, FLEXIBILITY, AND MASS CHARACTERISTICS*.

(F/D)	(L/D)	P_{Eu}/D (N/m)	P_{ℓ}/D (N/m)	$F_{lateral}$ (mm/N)	F_{axial} (mm/N)	Mass/$(\pi D_2^2/4)$ (gm/m^2)
1/2	1.07	12.2	0.605	0.358	0.319	6.14
1	1.37	20.9	0.857	0.535	0.0797	11.1
2	2.21	22.7	1.22	1.59	0.0512	25.4

*Buckling loads are for axially loaded individual columns. Flexibility coefficients are for tripod assembly assuming a rigid reflector. Material parameters: $E = 1.1 \times 10^{11}$ N/m^2, $\rho = 1520$ kg/m^3, $t = 0.35$ mm, $(w_{rms}/D) = 10^{-5}$. ℓ/D and d/D given in Table 3-1. Fitting mass factor, $k = 2$.

Under these assumptions, the reflector-only unit masses were found to be approximately 130 gm/m^2 for all three considered (F/D) values for the geodesic dome configuration and approximately 400 gm/m^2 for the tetrahedral truss configuration. Since these unit masses are much larger than those reported in Tables 3-1 and 3-2 for solid tube designs, no further consideration was given to the inflated strut concept.

REFERENCES

3-1. Hedgepeth, J.M.: Influence of Interorbit Accleration on the Design of Large Space Antennas. NASA Conference Publication 2144, May 1980.

3-2. Hedgepeth, J.M.: Critical Requirements for the Design of Large Space Structures. ARC-R-1016, Astro Research Corporation, 9 September 1981.

3-3. Miller, R.K.; Adams, L.R.; and Hedgepeth, J.M.: Structural Concepts for Ultralightweight Spacecraft. ARC-TN-1104, Astro Research Corporation, 1 June 1981.

SECTION 4
MASS SUMMARY AND COMPARISON OF DESIGNS

Presented in this section is a summary of the unit masses for paraboloidal reflector structures obtained by three very different design approaches. These approaches include (1) An entirely inflated membrane configuration, (2) a spin-stiffened configuration, and (3) A truss-supported configuration. The spin-stiffened and truss-supported configurations are described in more detail in Sections 2 and 3 of this report whereas the entirely inflated configuration is described in a previous report (Ref. 4-1) and is described briefly in what follows.

Also presented herein is a discussion and comparison of the strengths and weaknesses of the three basic design configurations.

4.1 MASS SUMMARY FOR AN INFLATED REFLECTOR SPACECRAFT

Consider an inflated paraboloidal reflector consisting basically of a paraboloidal membrane surface joined at its outer rim to a conical membrane surface as shown in Figure 4-1. The conical membrane is assumed to be transparent to the radiation of interest while the paraboloid is coated with a reflective material. As discussed in Reference 4-1, the tension fields induced in the membrane surfaces due to internal pressurization and the abrupt change in direction of these tension forces at the rim (cone/paraboloid junction) necessitate special attention to load transfer at the rim. Specifically, to avoid the development of substantial wrinkle regions in the paraboloid near the rim, a separate compression-carrying rim structural component is necessary. For the design developed in Reference 4-1, this compression rim was considered to be a segmented ring composed of many short segments, each of which is straight. Furthermore, each rim segment was assumed to be a separately inflated (noncylindrical) isotensoid column as shown in Figure 4-2 and discussed in Reference 4-1. Attachment between the rim and membrane surfaces occurs only at the junctions between straight rim segments as shown in Figure 4-3. Load transfer between the membrane surfaces and rim is provided by a scalloped arrangement of arched edge tendons which

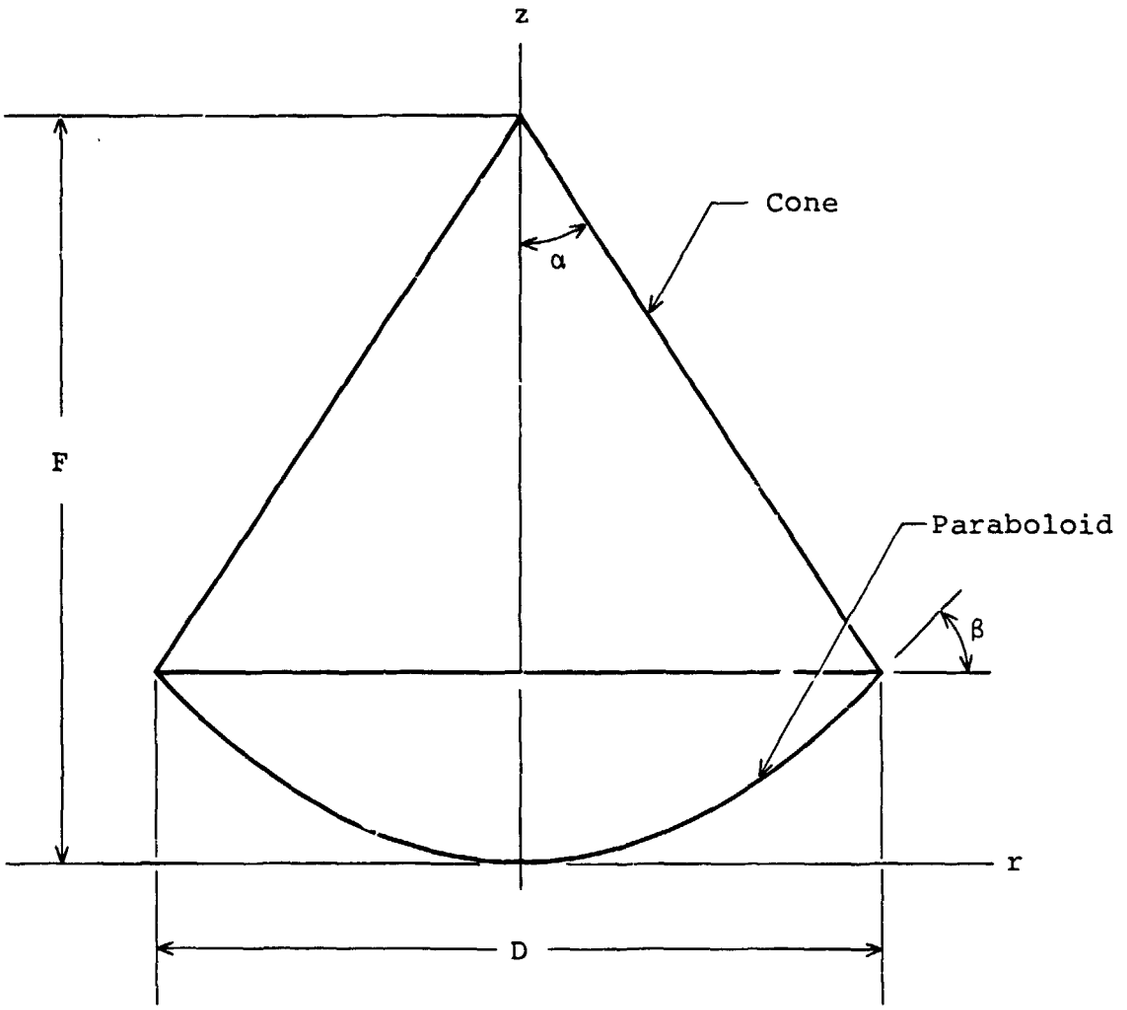

Figure 4-1. Geometry of cone-paraboloid reflector spacecraft. *112A*

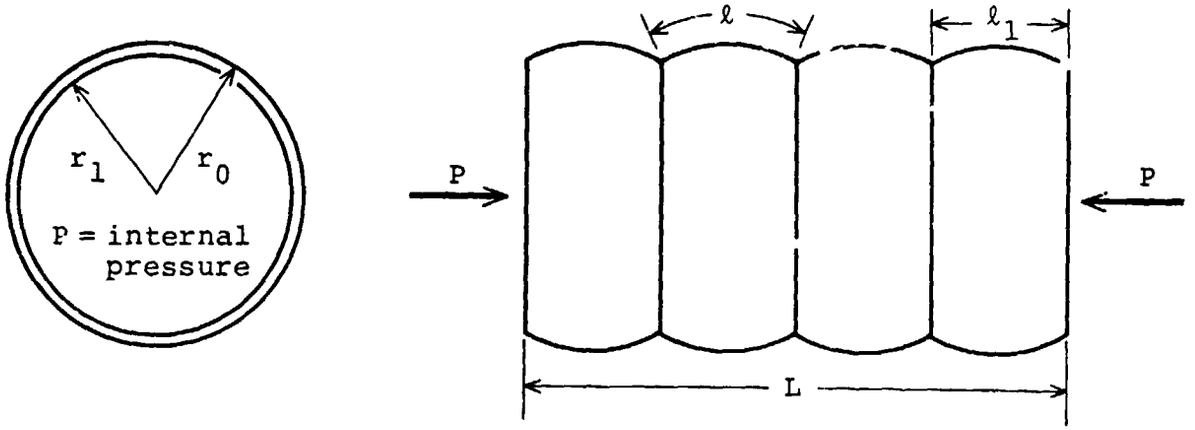

$$L < L_{CRIT} = r_1 - f\left(\frac{\ell}{r_1}, \frac{P}{\pi r_1^2 p}\right)$$

Figure 4-2. Pressurized isotensoid strut used in segmented compression rim of inflated cone/paraboloid reflector. *113A*

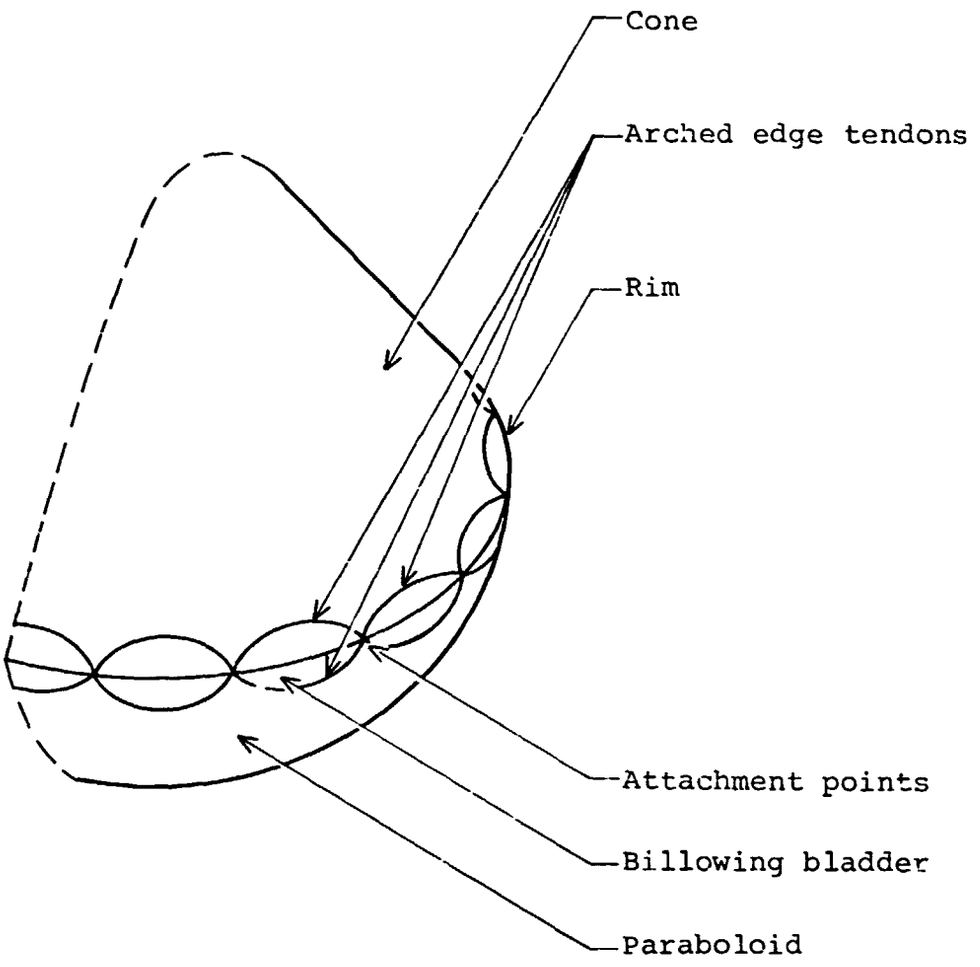

Figure 4-3. Detail of load path between membrane and rim attachment points for inflated reflector configuration. *114A*

are bonded directly to the edge of the membrane and made of the same material. Leakage of pressurant at the rim is prevented by a (nonstructural) billowing bladder.

The design of this inflated configuration was governed by setting the maximum edge loading in the membrane surfaces equal to an arbitrarily chosen predetermined value of 20 N/m, corresponding to a maximum working stress of 1×10^7 N/m^2 in a membrane of thickness 2×10^{-6} m. For a material of Kapton polymer film, the working stress is well below the ultimate strength of the material, but prolonged loading at higher stress levels may cause significant creep.

As a result of setting the maximum edge tension to a predetermined value under static pressurization, the necessary internal pressure and variation in membrane stresses over the surface may be obtained. It is found that the maximum membrane stress always occurs near the reflector rim and that the membrane stresses near the apex of the cone (feed of the paraboloid) are always zero regardless of the amount of internal pressure used. The pressurant was assumed to be N_2 at 300 K.

Next, the forces in the arched edge tendons were determined from an assumed circular arc geometry of the tendons. From these edge tendon forces, the compression force carried by each rim segment was inferred. The edge tendons are sized by assuming that they are made of the same material as the membrane and that they have the same working stress. The rim segments are designed on the basis of an analysis of the buckling load of individual rim segments, assuming a safety factor of two and ignoring the effects of initial imperfections in the column. The pressurant used in the inflated isotensoid column segments is N_2 gas at 300 K. The column reinforcing material was chosen as Kevlar 49 fiber with density $\rho_f = 1380$ kg/m^3 and working stress of $\sigma_t = 6.9 \times 10^8$ N/m^2.

The mass of each major structural component of the inflated reflector spacecraft is reviewed in the following paragraphs, and for the particular (F/D) values chosen, numerical results are presented in Table 4-1.

TABLE 4-1. COMPARISON OF STRUCTURAL MASSES OF THREE PARABOLOIDAL REFLECTOR SPACECRAFT CONFIGURATIONS.

CONFIGURATION AND COMPONENT	MASS/($\pi D^2/4$), g/m^2		
	F/D = 1/2	F/D = 1	F/D = 2
Inflated Configuration			
Membrane	9.53	12.8	20.4
Pressurant	0.0505	0.0706	0.0737
Deep-arc tendons	0.514	0.527	0.488
Inflated isotensoid rim	2.06	2.06	2.06
Total	12.2	15.5	23.0
Spinning Configuration			
Membrane	4.24	4.06	4.02
Outer rim mass	0.298	0.200	0.181
Front and back stays	0.00746	0.00596	0.00568
Inflated center column	0.169	0.550	3.53
Total	4.71	4.82	7.74
Total with control-designed column	5.12	5.91	14.01
Truss Configuration			
Tetrahedral truss	124	119	117
Mesh/membrane	4.24	4.06	4.02
Tripod	6.14	11.1	25.4
Total	134	134	146
Geodesic dome	39.3	37.7	37.1
Ring stiffener	16.0	21.7	30.2
Mesh/membrane	4.24	4.06	4.02
Tripod	6.14	11.1	25.4
Total	65.7	74.6	96.7

4.1.1 Membrane

The membrane mass is the product of the total surface area of membrane material, the membrane thickness, and the mass density. Thus,

$$M_{membrane} = \rho t A \qquad (4\text{-}1)$$

where

A = membrane surface area, $(\sim D^2)$

ρ = mass density

t = membrane thickness

For the results presented in Table 4-1, $\rho = 2 \times 10^3$ kg/m^3 and $t = 2 \times 10^{-6}$ m. The term A is a function of (F/D) as given in Eq. (2-5) of Reference 4-1.

4.1.2 Pressurant

The pressurant mass is the product of the mass density ρ of the pressurant and the total volume of pressurant. However, for N_2 at 300 K, the mass density is proportional to the pressure which, in this design, is proportional to the maximum allowable edge tension T_{max} in the membrane. Thus,

$$M_{pressurant} = \rho V \propto T_{max} D^2 \qquad (4\text{-}2)$$

where

T_{max} = maximum allowable edge tension

V = volume of pressurant, $\sim D^3$

For the results presented in Table 4-1, T_{max} = 20 N/m. The terms V and ρ are functions of (F/D) through Eqs. (2-7), (2-8), (2-16), and (2-17) of Reference 4-1.

4.1.3 Deep-Arc Tendons

The tendon mass is the product of the mass density ρ, the total tendon length L, and the cross-sectional area A. However, the required cross-sectional area for a given working stress σ may be related back to the allowable edge tension T_{max}. Thus, it may be shown that

$$M_{tendons} \propto \frac{T_{max} D^2 \rho}{\sigma} \tag{4-3}$$

where

T_{max} = maximum allowable edge tension

σ = working stress in tendons

ρ = mass density of tendons

The mass is also dependent on the ratio (F/D) through Eqs. (2-20), (2-27), (2-28), (2-7), and others. For the results presented in Table 4-1, $\rho = 2 \times 10^3$ kg/m^3, $T_{max} = 20$ N/m, and $\sigma = 1 \times 10^7$ N/m.

4.1.4 Inflated Rim

The mass of the inflated rim is the product of the overall mass density of the wall and pressurant of column material and the volume occupied by the inflated rim as given in Eq. (2-61) of Reference 4-1. The parameters are not involved in a simple manner, and no attempt will be made here to parameterize these results, except that

$$M_{rim} \propto PD \propto T_{max} D^2 \tag{4-4}$$

where

T_{max} = maximum allowable edge tension

The value of T_{max} used to obtain the results presented in Table 4-1 is 20 N/m.

4.1.5 Strengths and Weaknesses of the Design

Compared with the other configurations, it is seen that the inflated spacecraft is much lighter than the truss spacecraft but not as light as the spinning spacecraft. The inflated spacecraft has the potential advantage of an obvious and reliable deployment mechanism and a potentially high packaging efficiency.

Potential disadvantages of the inflated configuration include leakage of pressurant and susceptibility to meteoroid puncture, inherently low stiffness of the membrane wall near the apex (feed) of the cone, and potentially large errors in surface accuracy.

4.2 MASS SUMMARY OF A SPINNING REFLECTOR SPACECRAFT

A detailed discussion of the design procedures used to develop the dimensions and masses of spacecraft structural components for the spinning configuration are given in Section 2 of this report. Consequently, what follows is a review of the parameters which affect the mass of each major structural component. Numerical values are presented in Table 4-1 for comparison with other configurations.

4.2.1 Membrane

The mass of the membrane surface is the product of the mass density ρ, the membrane thickness t, and the surface A. Thus,

$$M_{membrane} = \rho t A \qquad (4\text{-}5)$$

For the results presented in Table 4-1, $\rho = 2 \times 10^{3}$ kg/m^{3}, $t = 2 \times 10^{-6}$ m, and A is the sum of paraboloidal and conical areas which depend on (F/D).

4.2.2 Outer-Rim Mass

The mass of the outer rim is the product of the circumference πD of the rim and the lineal mass density $\hat{m}$ of the added rim mass. Thus,

$$M_{outer\ rim} = \hat{m}\pi D \qquad (4\text{-}6)$$

From Eqs. (2-21) through (2-24), we find that

$$\hat{m} \propto N_{\phi}(r = D/2)/\omega^2 \tag{4-7}$$

However, N_{ϕ} and ω^2 are not conveniently parameterized. It may be shown that

$$M_{\text{outer rim}} \propto \frac{N_{\phi_{max}} \rho t D^2}{N_{\theta_{min}} + N_{\phi_{max}} f_1} \tag{4-8}$$

where

$N_{\phi_{max}}$ = arbitrarily chosen maximum N_{ϕ} at r = 0.2 D

$N_{\theta_{min}}$ = arbitrarily chosen minimum N_{θ} at r = 0.2 D

ρ = mass density of membrane

t = membrane thickness

f_1 = function of (F/D) = $\left[1 + (D/10\ F)^2\right]^{-1}$

For the results presented in Table 4-1, $N_{\phi_{max}}$ = 5 N/m, $N_{\theta_{min}}$ = 0.85 N/m, ρ = 2×10^3 kg/m^3, and t = 2×10^{-6} m.

4.2.3 Front and Back Stays

The mass of the front and back stays may be characterized as

$$M_{\text{stays}} \propto \frac{\rho N_{\phi_{max}}}{\sigma} \tag{4-9}$$

where

ρ = mass density of stays

σ = working stress of stays

$N_{\phi_{max}}$ = arbitrarily chosen maximum N_ϕ at r = 0.2 D

For the results presented in Table 4-1, $N_{\phi_{max}}$ = 5 N/m, ρ = 1380 kg/m^3, and σ = 6.9 x 10^8 N/m^2 for a stay material of Kevlar 49.

4.2.4 Inflated Center Column

The mass of the inflated center column is given by Eq. (2-34). It is not easily parameterized since it is dependent upon numerical solutions to a cubic equation for the required column radius r.

4.2.5 Strengths and Weaknesses of the Design

From Table 4-1, it is observed that the spinning configuration is significantly lighter than any of the competing configurations. Another potential advantage is that the centrifugal force may be used in a reliable deployment mechanism.

The spinning configuration presents a number of potential disadvantages which are inherent by products of rotational motion. First of all, the angular momentum of a large rotating spacecraft is quite large and provides an impediment to maneuvers which require significant motion of the axis. As previously discussed, it may be necessary to add a large counter-rotating flywheel to cancel the spacecraft angular momentum and provide a means for attitude control. However, such a flywheel would amplify whirl instability considerations in the design of the central column, resulting in larger total spacecraft mass, as shown in Table 4-1, under the heading "total with control-designed column." In addition to angular momentum effects, the spacecraft must be dynamically balanced by adding masses in appropriate locations in order that the spin axis becomes the principle axis of inertia. As previously shown, the designs presented in Table 4-1 have not been dynamically balanced, and therefore additional masses will be required. Finally, the spinning configuration provides an opportunity for a plethora of dynamic instabilities which should be investigated.

4.3 MASS SUMMARY FOR A TRUSS REFLECTOR SPACECRAFT

A detailed discussion of the design procedures used to develop the dimensions and masses of spacecraft structural components for the truss configurations are given in Section 3 of this report. Consequently, what follows is a review of the parameters which affect the mass of each major structural component. Numerical values are presented in Table 4-1 for comparison with other configurations.

4.3.1 Tetrahedral Truss

The mass of the deep tetrahedral truss may be characterized as

$$M_{tetra} \propto \rho D^2 N^{1/3} t^{2/3} E^{-1/3} \qquad (4\text{-}10)$$

where

ρ = mass density of truss member material

N = edge tension in mesh supported by truss

t = wall thickness of truss members

E = modulus of elasticity of truss members

For the results presented in Table 4-1, ρ = 1520 kg/m^3, E = 1.1 x 10^{11} N/m^2 for graphite/epoxy material, t = 0.35 mm, and N = 1 N.

4.3.2 Geodesic Dome

The mass of the simple geodesic dome may also be characterized by Eq. (4-10).

4.3.3 Ring Stiffener

The mass of the ring stiffener for the geodesic dome may be characterized as

$$M_{ring} \propto \sqrt{\frac{w_{rms}}{D}}\, \rho D^2 N^{1/3} t^{2/3} E^{-1/3} \qquad (4\text{-}11)$$

where ρ, N, t, and E are as described above, and w_{rms} is the allowable facet-flattening error in the reflective surface. For the results presented in Table 4-1, $w_{rms}/D = 10^{-5}$.

4.3.4 Mesh/Membrane

The mass of the mesh or membrane reflective surface supported by the truss may be characterized as

$$M_{mesh} \propto m'D^2 \qquad (4\text{-}12)$$

where m' is the mass per unit area of the mesh material. For the results presented in Table 4-1, $m' = 4\ g/m^2$.

4.3.5 Tripod

The mass of the tripod may be characterized as

$$M_{tripod} \propto N^{1/3}\, t^{-1/3}\, E^{-1/3} \sqrt{\frac{w_{rms}}{D}} \qquad (4\text{-}13)$$

where N, t, E and (w_{rms}/D) are as described above. The values for these quantities which were used in constructing Table 4-1 are also presented above.

4.3.6 Strengths and Weaknesses of the Design

Both of the truss configurations are substantially heavier than the other two competing designs. Furthermore, the packaging efficiency and deployment procedures for each are not likely to be as favorable as those for the competing designs. However, the tetrahedral truss has a significant advantage in that precision design and fabrication procedures provide the opportunity for a relatively high surface accuracy. It may be that the dome structure is capable of a surface accuracy below that of the tetrahedral truss but above that of the other two competing designs.

REFERENCES

4-1. Hedgepeth, J.M.; and Miller, R.K.: Final Report - A Study of Structural Concepts for Ultralightweight Spacecraft. Astro Research Corporation, ARC-TN-1114, 14 July 1982.

APPENDIX
VIBRATIONS OF A SHALLOW DOME

For a shallow spherical come ($r = a\phi$) we can ignore the effects of in-surface acceleration loads. We get

$$\frac{\partial N_r}{\partial r} + \frac{1}{r}\frac{\partial N_{r\theta}}{\partial \theta} + \frac{N_r - N_\theta}{r} = 0$$

$$r\frac{\partial N_\theta}{\partial \theta} + \frac{\partial}{\partial r}\left(r^2 N_{r\theta}\right) = 0$$

$$N_r + N_\theta = ma\omega^2 w$$

Rewriting gives

$$N_r + N_\theta = \frac{Et}{(1-\nu)}\left(\frac{\partial u}{\partial r} + \frac{u}{r} + \frac{1}{r}\frac{\partial v}{\partial \theta} + \frac{2w}{a}\right)$$

$$N_r - N_\theta = \frac{Et}{1+\nu}\left(\frac{\partial u}{\partial r} - \frac{u}{r} - \frac{1}{r}\frac{\partial v}{\partial \theta}\right)$$

$$N_{r\theta} = \frac{Et}{2(1+\nu)}\left(\frac{1}{r}\frac{\partial u}{\partial \theta} + \frac{\partial v}{\partial r} - \frac{v}{r}\right)$$

The first two of the equilibrium equations are satisfied by relating the stresses to the stress potential Φ, where

$$N_r = -\frac{1}{r}\frac{\partial \Phi}{\partial r} - \frac{1}{r^2}\frac{\partial^2 \Phi}{\partial \theta^2}$$

$$N_\theta = -\frac{\partial^2 \Phi}{\partial r^2}$$

$$N_{r\theta} = \frac{\partial}{\partial r}\left(\frac{1}{r}\frac{\partial \Phi}{\partial \theta}\right)$$

Manipulating the second and third stress-displacement relations yields

$$\nabla^2\left(\frac{u}{r}\right) = \frac{1+\nu}{Et}\left[\frac{1}{r}\frac{\partial}{\partial r}(N_r - N_\theta) + \frac{2}{r^2}\frac{\partial N_{r\theta}}{\partial \theta}\right]$$

$$\nabla^2\left(\frac{v}{r}\right) = \frac{1+\nu}{Et}\left[\frac{2}{r}\frac{\partial N_{r\theta}}{\partial r} - \frac{1}{r^2}\frac{\partial}{\partial \theta}(N_r - N_\theta)\right]$$

where

$$\nabla^2 = \frac{\partial^2}{\partial r^2} + \frac{1}{r}\frac{\partial}{\partial r} + \frac{1}{r^2}\frac{\partial^2}{\partial \theta^2}$$

is the usual Laplacian.

Taking the Laplacian of the first of the stress-displacement relations gives

$$\frac{1-\nu}{Et}\nabla^2(N_r + N_\theta) = -\frac{1+\nu}{Et}\nabla^2(N_r + N_\theta) + \frac{2}{a}\nabla^2 w$$

Thus

$$\nabla^2\left[w - \frac{a}{Et}(N_r + N_\theta)\right] = 0$$

Substituting from the third equilibrium equation finally gives

$$\left(1 - \frac{ma^2\omega^2}{Et}\right)\nabla^2 w = 0$$

Either

$$\omega^2 = \frac{Et}{ma^2}$$

or

$$\nabla^2 w = 0$$

If we require w = 0 at the boundary r = D/2, then no nontrivial solution exists with a zero Laplacian. Therefore, for supported edges, a shallow spherical (or paraboloidal) dome would exhibit many vibration modes, all having the same vibration frequency.

If the rim is allowed to distort, then other frequencies are possible. We would like to determine how stiff the rim-reinforcing ring must be in order to ensure that the other frequencies are higher than the basic one above.

Let the deformation be sinusoidal around the circumference; that is

$$w = w_n \cos n\theta$$

and so forth.

The nonsingular solution with a zero Laplacian is

$$w_n = W\left(\frac{2r}{D}\right)^n$$

In terms of the stress potential, the third equilibrium equation gives

$$\nabla^2\Phi = -ma\omega^2 W\left(\frac{r}{a}\right)^n \cos n\theta$$

The general solution is

$$\Phi_n = \left\{F\left(\frac{2r}{D}\right)^n - \frac{ma\omega^2 W}{4(n+1)}\left(\frac{2r}{D}\right)^{n+2}\left(\frac{D}{2}\right)^2\right\}\cos n\theta$$

The stresses are

$$N_r = \left[n(n-1)\frac{4F}{D^2}\left(\frac{2r}{D}\right)^{n-2} - \frac{n-2}{4}ma\omega^2 W\left(\frac{2r}{D}\right)^n\right]\cos n\theta$$

$$N_\theta = \left[-n(n-1)\frac{4F}{D^2}\left(\frac{2r}{D}\right)^{n-2} + \frac{n+2}{4}ma\omega^2 W\left(\frac{2r}{D}\right)^n\right]\cos n\theta$$

$$N_{r\theta} = -n\left[(n-1)\frac{4F}{D^2}\left(\frac{2r}{D}\right)^{n-2} - \frac{ma\omega^2 W}{4}\left(\frac{2r}{D}\right)^{n}\right]\sin n\theta$$

With regard to the u and v displacements, note that

$$\frac{\partial u}{\partial r} = \varepsilon_r - \frac{W}{a}$$

Therefore

$$\frac{\partial u}{\partial r} = -\frac{W}{a} + \frac{N_r - \nu N_\theta}{Et}$$

$$= \left\{\frac{(1+\nu)}{Et} n(n-1)\frac{4F}{D^2}\left(\frac{2r}{D}\right)^{n-2} - \left[\frac{(1+\nu)n-2(1-\nu)}{4}\frac{ma^2\omega^2}{Et} + 1\right]\frac{W}{a}\left(\frac{2r}{D}\right)^{n}\right\}\cos n\theta$$

Integrating, and noting that $u(0,\theta) = 0$ for $n \neq 1$, gives

$$u = \left\{\frac{(1+\nu)}{Et} n \frac{F}{D}\left(\frac{2r}{D}\right)^{n-1} - \frac{D}{2(n+1)}\left[\frac{(1+\nu)n-2(1-\nu)}{4}\frac{ma^2\omega^2}{Et} + 1\right]\frac{W}{a}\left(\frac{2r}{D}\right)^{n+1}\right\}\cos n\theta$$

Similarly

$$\frac{\partial}{\partial\theta} = -u - r\frac{W}{a} + r\frac{N_\theta - \nu N_r}{Et}$$

So

$$v = \left\{-\frac{(1+\nu)}{Et} n \frac{2F}{D}\left(\frac{2r}{D}\right)^{n-1} + \frac{D}{2(n+}\left[\frac{(1+\nu)n+4}{4}\frac{ma^2\omega^2}{Et} - 1\right]\frac{W}{a}\left(\frac{2r}{D}\right)^{n+1}\right\}\sin n\theta$$

Inasmuch as we are dealing with a membrane, we cannot expect to enforce compatibility of edge deflections normal to the membrane. We must, however, require that the u and v deflections match those of a supporting ring.

Let the u and v displacements at r = D/2 be

$$u = U \cos n\theta$$

$$v = V \sin n\theta$$

The

$$U + V = \frac{D}{2(n+1)} \left[\frac{4+2(1-\nu)}{4} \frac{ma^2\omega^2}{Et} - 2 \right] \frac{W}{a}$$

Thus

$$W = \frac{(n+1)a}{D} \frac{U + V}{\frac{3-\nu}{4} \frac{ma^2\omega^2}{Et} - 1}$$

Solving for F gives

$$\frac{4F}{D^2} = \frac{Et}{nD} \left[\frac{U - V}{1+\nu} + \frac{n+1}{4} \frac{U + V}{\frac{3-\nu}{4} \frac{ma^2\omega^2}{Et} - 1} \frac{ma^2\omega^2}{Et} \right]$$

The resulting edge stresses are

$$N_r = \frac{Et}{D} \left[\frac{(n-1)}{1+\nu} (U - V) + \frac{n+1}{4} \frac{U + V}{\frac{3-\nu}{4} \frac{ma^2\omega^2}{Et} - 1} \frac{ma^2\omega^2}{Et} \right] \cos n\theta$$

$$N_{r\theta} = \frac{Et}{D} \left[\frac{(n-1)}{1+\nu} (V - U) + \frac{n+1}{4} \frac{ma^2\omega^2}{Et} \frac{U + V}{\frac{3-\nu}{4} \frac{ma^2\omega^2}{Et} - 1} \right] \sin n\theta$$

Let us write these in terms of radial, circumferential, and vertical coordinates $\bar{u}_1$, $\bar{u}_2$, and $\bar{u}_3$.

$$\bar{u}_1 = U + \frac{D}{2a} W$$

$$\bar{u}_2 = V$$

$$\bar{u}_3 = -\frac{D}{2a} U + W$$

$$U = \bar{u}_1 - \frac{D}{2a} \bar{u}_3$$

$$V = \bar{u}_2$$

Then

$$\frac{N_r}{\cos n\theta} = \frac{Et}{D}\left[\frac{n-1}{1+\nu}\left(\bar{u}_1 - \bar{u}_2 - \frac{D}{2a}\bar{u}_3\right) + \frac{n+1}{4}\frac{ma^2\omega^2}{Et}\,\frac{\bar{u}_1+\bar{u}_2-\frac{D}{2a}\bar{u}_3}{\frac{3-\nu}{4}\frac{ma^2\omega^2}{Et}-1}\right]$$

$$\frac{N_{r\theta}}{\sin n\theta} = \frac{Et}{D}\left[-\frac{n-1}{1+\nu}\left(\bar{u}_1 - \bar{u}_2 - \frac{D}{2a}\bar{u}_3\right) + \frac{n+1}{4}\frac{ma^2\omega^2}{Et}\,\frac{\bar{u}_1+\bar{u}_2-\frac{D}{2a}\bar{u}_3}{\frac{3-\nu}{4}\frac{ma^2\omega^2}{Et}-1}\right]$$

Ring Stiffness Equations

If we ignore torsion, the equations governing the deformations of an unpreloaded ring are taken from Reference 1-2 to be

$$A\bar{u} = \bar{p}$$

where

$$\bar{u} = \begin{vmatrix} \bar{u}_1 \\ \bar{u}_2 \\ \bar{u}_3 \end{vmatrix}$$

$$A = \frac{4}{D^2}\begin{bmatrix} \frac{4EI_1}{D^2}n^4 + EA & \frac{4EI_1}{D^2}n^3 + EAn & 0 \\ \frac{4EI_1}{D^2}n^3 + EAn & \frac{4EI_1}{D^2}n^2 + EAn^2 & 0 \\ 0 & 0 & \frac{4EI_2}{D^2}n^4 \end{bmatrix}$$

$$\bar{p} = \begin{vmatrix} -\frac{N_r\left(\frac{D}{2}\right)}{\cos n\theta} + m_R\omega^2\bar{u}_1 \\ -\frac{N_{r\theta}\left(\frac{D}{2}\right)}{\sin n\theta} + m_R\omega^2\bar{u}_2 \\ \frac{\frac{D}{2a}N_r\left(\frac{D}{2}\right)}{\cos n\theta} + m_R\omega^2\bar{u}_3 \end{vmatrix}$$

Combining the first two gives

$$\frac{4}{D^2}\begin{bmatrix} \frac{4EI_1}{D^2}(n^4 - n^2) & \frac{4EI_1}{D^2}(n^3 - n) & 0 \\ EA(n^2 - 1) & EA(n^3 - n) & 0 \\ 0 & 0 & \frac{4EI_2}{D^2}n^4 \end{bmatrix} \begin{vmatrix} \bar{u}_1 \\ \bar{u}_2 \\ \bar{u}_3 \end{vmatrix} = \begin{vmatrix} -\frac{N_r}{\cos n\theta} + \frac{1}{n}\frac{N_{r\theta}}{\sin n\theta} + m_R\omega^2\left(\bar{u}_1 - \frac{1}{nu_2}\right) \\ \frac{N_r}{\cos n\theta} + \frac{nN_{r\theta}}{\sin n\theta} + m_R\omega^2\left(n\bar{u}_2 - \bar{u}_1\right) \\ \frac{\frac{D}{2a}N_r\frac{D}{2}}{\cos} + m_R\omega^2\bar{u}_3 \end{vmatrix}$$

or

$$\frac{4}{D^2}\begin{bmatrix} \frac{4EI_1}{D^2}(n^4 - n^2) & 0 & 0 \\ 0 & EA(n^2 - 1) & 0 \\ 0 & 0 & \frac{4EI_2}{D^2} n^4 \end{bmatrix} \begin{vmatrix} n\bar{u}_1 + \bar{u}_2 \\ \bar{u}_1 + n\bar{u}_2 \\ \bar{u}_3 \end{vmatrix} = \begin{vmatrix} -\frac{nN_r}{\cos n\theta} + \frac{N_{r\theta}}{\sin n\theta} + m_R\omega^2\left(n\bar{u}_1 - \bar{u}_2\right) \\ \frac{N_r}{\cos n\theta} + \frac{nN_{r\theta}}{\sin n\theta} + m_R\omega^2\left(n\bar{u}_2 - \bar{u}_1\right) \\ \frac{\frac{D}{2a} N_r\left(\frac{D}{2}\right)}{\cos n\theta} + m_R\omega^2 \bar{u}_3 \end{vmatrix}$$

Let

$$x_1 = n\bar{u}_1 + \bar{u}_2$$

$$x_2 = \bar{u}_1 + n\bar{u}_2$$

Then

$$\bar{u}_1 = \frac{nx_1 - x_2}{n^2 - 1}$$

$$\bar{u}_2 = \frac{x_1 + nx_2}{n^2 - 1}$$

Also

$$\frac{N_r}{\cos n\theta} = \frac{Et}{D}\left[\frac{x_1 - x_2}{1+\nu} - \frac{n-1}{1-\nu}\frac{D}{2a}\bar{u}_3 + \frac{ma^2\omega^2}{4Et}\frac{x_1 + x_2 - (n+1)\frac{D}{2a}\bar{u}_3}{\frac{3-\nu}{4}\frac{ma^2\omega^2}{Et} - 1}\right]$$

$$\frac{N_{r\theta}}{\sin n\theta} = \frac{Et}{D}\left[-\frac{x_1 - x_2}{1+\nu} + \frac{n-1}{1+\nu}\frac{D}{2a}\bar{u}_3 + \frac{ma^2\omega^2}{4Et}\frac{x_1 + x_2 - (n+1)\frac{D}{2a}\bar{u}_3}{\frac{3-\nu}{4}\frac{ma^2\omega^2}{Et} - 1}\right]$$

So

$$\frac{N_{r\theta}}{\sin n\theta} - n\frac{N_r}{\cos n\theta} = \frac{Et}{D}\left[-\frac{n+1}{1+\nu}(x_1 - x_2) + \frac{n^2-1}{1-\nu}\frac{D}{2a}\bar{u}_3 + \frac{ma^2\omega^2}{4Et}\frac{-(n-1)(x_1+x_2) + (n^2-1)\frac{D}{2a}\bar{u}_3}{\frac{3-\nu}{4}\frac{ma^2\omega^2}{Et} - 1}\right]$$

$$\frac{N_r}{\cos n\theta} - n\frac{N_{r\theta}}{\sin n\theta} = \frac{Et}{D}\left[\frac{n+1}{1+\nu}(x_1 - x_2) - \frac{n^2-1}{1+\nu}\frac{D}{2a}\bar{u}_3 + \frac{ma^2\omega^2}{Et}\frac{-(n-1)(x_1+x_2) + (n^2-1)\frac{D}{2a}\bar{u}_3}{\frac{3-\nu}{4}\frac{ma^2\omega^2}{Et} - 1}\right]$$

In order to simplify, let EA be very large so that the second equation yields $x_2 = 0$. Also let $EI_1 = EI_2 = EI$ and $\nu = 1/3$. Then

$$\begin{bmatrix} \left(\frac{2}{D}\right)^4 EI(n^4 - n^2) - \frac{n^2+1}{n^2-1}m_R\omega^2 + \frac{Et}{D}\frac{3(n+1) - (3n+1)\frac{ma^2\omega^2}{Et}}{4 - \frac{8}{3}\frac{ma^2\omega^2}{Et}} & -\frac{Et}{D}\left(\frac{D}{2a}\right)(n^2-1)\frac{3\left(1-\frac{ma^2\omega^2}{Et}\right)}{4-\frac{8}{3}\frac{ma^2\omega^2}{Et}} \\ -\frac{Et}{D}\left(\frac{D}{2a}\right)\frac{3\left(1-\frac{ma^2\omega^2}{Et}\right)}{4-\frac{8}{3}\frac{ma^2\omega^2}{Et}} & \left(\frac{2}{D}\right)^4 EIn^4 - m_R\omega^2 + \frac{Et}{D}\left(\frac{D}{2a}\right)^2\frac{3(n-1) - (3n-1)\frac{ma^2\omega^2}{Et}}{4-\frac{8}{3}\frac{ma^2\omega^2}{Et}} \end{bmatrix} \begin{vmatrix} x \\ \bar{u}_3 \end{vmatrix} = \begin{vmatrix} 0 \\ 0 \end{vmatrix}$$

Expanding the determinant gives the condition for nontrivial solution. This would allow the determination of the required ring stiffness to produce a desired frequency. Of course, we want to find the ring stiffness for which the frequency is the same as the fixed-edge value. Therefore, we set

$$\omega^2 = \frac{Et}{ma^2}$$

The result is

$$\left(\frac{2}{D}\right)^4 EIn^4 - \frac{m_R Et}{ma^2} - \frac{3}{2}\left(\frac{D}{2a}\right)^2\frac{Et}{D} = 0$$

The highest stiffness arises from n=2. Solving gives, finally

$$EI = \left(\frac{D}{2a}\right)^2 \frac{EtD^3}{256}\left(\frac{3}{2} + \frac{M_R}{M_S}\right)$$

where M_R and M_S are the masses of the ring and the surface, respectively.